HYDROSTATIC PRESSURE RETAINMENT

A thesis presented to

the faculty of the

Fritz J. and Dolores Russ
College of Engineering and Technology
of
Ohio University

In partial Fulfillment

Of the requirements for the Degree

Master of Science

Robert J. Setlock, Jr.

June 2004

This thesis entitled

HYDROSTATIC PRESSURE RETAINMENT

by Robert J. Setlock, Jr.

has been approved

for the Department of Mechanical Engineering

and the Russ College of Engineering and Technology

Bhavin V. Mehta
Associate Professor
Department of Mechanical Engineering

R. Dennis Irwin
Dean, Fritz J. and Dolores H. Russ
College of Engineering and Technology

SETLOCK, ROBERT J., JR. M.S. June 2004. Mechanical Engineering

Hydrostatic Pressure Retainment (107pp.)

Director of Thesis: Bhavin V. Mehta

There is a great deal of attention being concentrated on reducing the weight of pressure vessels and fuel/oxidizer tanks (tankage) by 10% to 20%. Most efforts are focused at the use of new lighter weight high strength materials to achieve this goal. This author proposes another approach called Hydrostatic Pressure Retainment™ (HPR™) which has the potential of reducing tank weights by nearly 40% while simultaneously increasing safety and design versatility. HPR™ is an original invention of the author and his advisor, and represents a truly novel approach to light weight pressure vessel design. Described herein are the initial steps towards development of this new technology.

Approved: Bhavin V. Mehta
Associate Professor of Mechanical Engineering

TABLE OF CONTENTS

LIST OF FIGURES

LIST OF TABLES

CHAPTER 1. INTRODUCTION

Hydrostatic Pressure Retainment (HPR™) is a new invention useful for designing and manufacturing pressure vessels composed of any homogeneous, isotropic structural material. HPR™ allows pressure vessels to fabricated into any size and any shape, while simultaneously retaining very high structural efficiencies. Therefore, HPR™ pressure vessels are particularly well suited for applications where size, shape, and weight limitations are important, such as automotive hydrogen storage.

An examination of a traditional spherical shell pressure vessel reveals that the structural material is subjected to bi-axial or planar stress equal in both planar directions when pressure is applied to the vessel. The one direction, which is perpendicular to a plane tangent to any point on the surface of the sphere, is not under any measurable stress (assume a thin shell vessel). Therefore, in a spherical shell, when the two equal stresses in the planar directions reach the yield stress, the stress in the perpendicular direction is still zero. So, a spherical shell pressure vessel can be considered 67% efficient in the use of available structural material (Figure 1.1). Note: {(100% + 100% + 0%) / 3 = 67%}

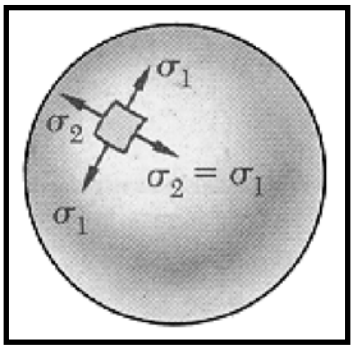

Figure 1.1: Bi-Axial Planar Stress where ($\sigma_1 = \sigma_2$)

An examination of a traditional cylindrical shell pressure vessel reveals that the structural material (in the cylinder portion) is subjected to bi-axial or planar stress where the stress in the hoop direction is always twice the stress in the longitudinal direction when pressure is applied to the vessel. The one direction, which is perpendicular to a plane tangent to any point on the surface of the cylinder, is not under any measurable stress (assume a thin shell vessel). Therefore, in a cylindrical shell, when the stress in the hoop direction reaches the yield stress, the stress in the longitudinal direction is only half of the yield stress, and the stress in the perpendicular direction is zero. So, a cylindrical shell pressure vessel can be considered 50% efficient in the use of available structural material (Figure 1.2). Note: {(100% + 50% + 0%) / 3 = 50%}

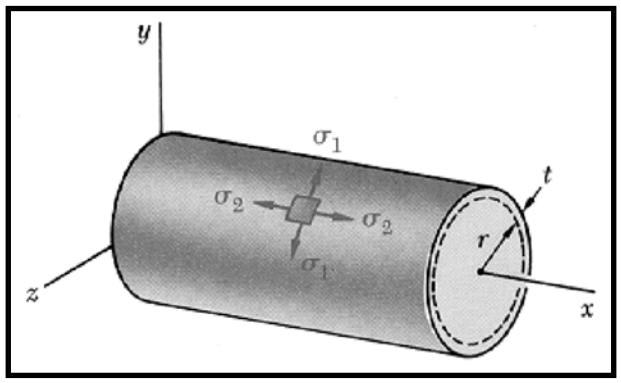

Figure 1.2: Bi-Axial Planar Stress where ($\sigma_1 = 2\sigma_2$)

HPR™ involves the use of an inner matrix as the structural support as opposed to the traditional use of an outer shell as the structural support. In order to perform with equal or better structural efficiency as a traditional outer shell arrangement, an HPR™ inner matrix arrangement must incorporate a particular morphology (shape of the inner details) which subjects a large portion of the structural material to tri-axial or hydrostatic

tensile stress when pressure is applied to the vessel. Therefore, with an ideal HPR™ inner matrix, when stress in any direction reaches the yield stress, the stress in the other directions will also equal the yield stress. This results in a nearly 100% efficient use of the structural material. It also results in a minimized development of internal shears as a result of the near equal omni-directional characteristic of the stresses (Figure 1.3). Note: {(100% + 100% + 100%) / 3 = 100%}

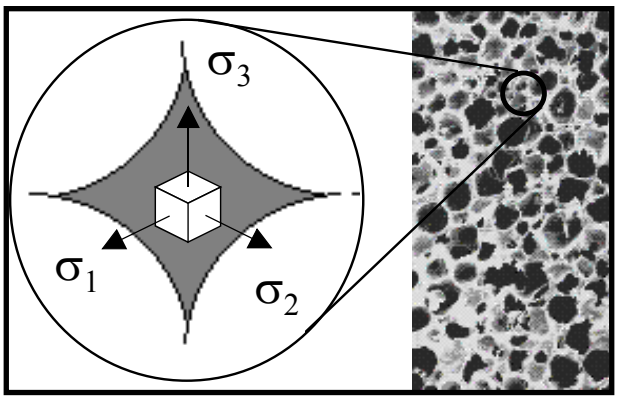

Figure 1.3: Tri-Axial Hydrostatic Stress where ($\sigma_1 = \sigma_2 = \sigma_3$)

Accordingly, if one is careful to ensure a consistent and proper morphology, the inner matrix approach can be more structurally efficient that either spherical shells or cylindrical shells. Actual practice (with metal foam samples produced at Fraunhofer USA Laboratories) has shown that it is reasonable to approach and meet 80% structural efficiency with HPR™ inner matrix pressure vessels.

1.1 Detailed Description

Use of a tensely stressed inner matrix as the principle load bearing component in a pressure vessel offers an opportunity to optimize (minimize) material usage. This

optimization is best accomplished when a homogeneous isotropic parent material is expanded to the lower density matrix, and when the resulting matrix retains all or most of the homogeneous isotropic qualities. This is because an inner matrix will be stressed equally in all three planes (hydrostatic tension).

For the purposes of this comparison we shall consider inner matrices that are composed of homogeneous isotropic parent materials. These inner matrices shall be assumed to have relative densities between 2% -30%, thus allowing between 70% - 98% of useful storage volume within the pressure vessel body. Depending upon the method of fabrication, the expanded matrix may retain all or some of the homogeneous isotropic qualities of the parent material.

If all the homogeneous isotropic qualities are retained after expanding (Figures 1.4 and 1.5 [1]) the parent material to the lower density matrix (best case), the strength of the expanded matrix will vary linearly with its relative density. In this case, $\sigma_{foam}/\sigma_{solid} = \rho_{foam}/\rho_{solid}$ where σ = stress, and ρ = density. Therefore, the density requirement for such an inner matrix is simply equal to the ratio of the required hydrostatic tensile strength (maximum pressure to be stored) over the hydrostatic tensile strength for the parent material (including the factor of safety). Because an inner matrix will be equally stressed in all three planes, hydrostatic tensile strength, which generally exceeds axial tensile strength, is the appropriate measure. However, if some or all of the homogeneous isotropic qualities were lost due to imperfect expansion of the parent material to the lower density matrix, a higher density inner matrix would be required.

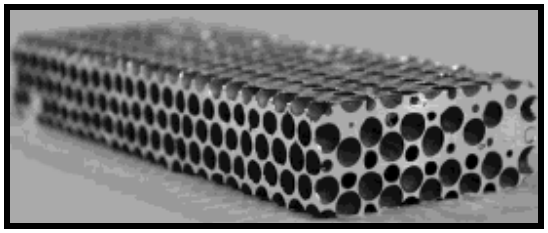

Figure 1.4: A Closed Cell Foam Provides an Ideal Microstructure [1]

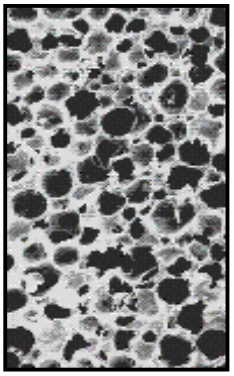

Figure 1.5: A Nearly Closed Cell Foam Provides an Almost Ideal Microstructure [1]

Consider a poor-case expansion where all homogeneous isotropic qualities are lost (Figure 1.6 [2]) and the resulting matrix is composed of pure axial (one dimensional) supports (similar to wires or fibers). In this case, $\sigma_{foam}/\sigma_{solid} = 0.333(\rho_{foam}/\rho_{solid})^{3/2}$. Therefore, the strength of a poor-case matrix would be considerably less than that of the best-case matrix.

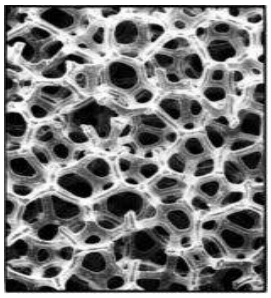

Figure 1.6: Open Cell Foam Microstructure Degraded to Simple Axial Members [2]

In Summary:

Best Case (Ideal) Matrix Expansion (All homogeneous isotropic qualities retained)	$\sigma_{foam}/\sigma_{solid} = \rho_{foam}/\rho_{solid}$
Poor Case Matrix Expansion (All homogeneous isotropic qualities lost)	$\sigma_{foam}/\sigma_{solid} = 0.333(\rho_{foam}/\rho_{solid})^{3/2}$ $\Longrightarrow \sigma_{foam}/\sigma_{solid} << (\rho_{foam}/\rho_{solid})$

Table 1.1: Best Case (Ideal) Matrix Expansion vs. Poor Case Matrix Expansion

1.2 Material Efficiency Comparison: Conventional Outer Shell .vs. Inner Matrix

1.2.1 Spherical Shell Comparison

A simple exercise reveals a relationship that describes the volume of structural material required to fabricate a conventional spherical pressure vessel that incorporates a traditional outer shell. The volume of structural material required is a function of the size (radius) of the pressure vessel, the maximum pressure to be stored, and the strength properties of the material selected for fabrication of the outer shell (maximum allowable stress).

Recall for thin walled spherical pressure vessels, Maximum Stress (Figure 1.7):

$$\sigma_{max} = \sigma_1 = \sigma_2 = pr/2t$$

which can be restated in terms of required thickness as:

$$t = pr/2\sigma_{max}$$

Where p = pressure, r = pressure vessel radius, and t = required wall thickness.

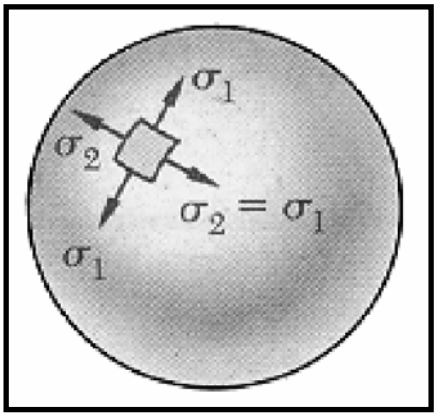

Figure 1.7: Thin Walled Spherical Shell

For a thin walled spherical pressure vessel, the volume of structural material required can be approximated by the product of the spherical surface area ($a = 4\pi r^2$) times the wall thickness (t). $V_{mtl} = at = 4\pi r^2 t$

Where V_{mtl} = volume of structural material, and a = surface area.

Which can be combined with the previous formula ($t = pr/2\sigma_{max}$) to obtain:

$$V_{mtl} = 2\pi r^3 p/\sigma_{max}$$

1.2.2 Spherical Inner Matrix

Again a simple exercise reveals a relationship that describes the volume of material required to fabricate a spherical pressure vessel that incorporates an inner matrix

(see Figure 1.8). Once more the volume of material required is a function of the size (radius) of the pressure vessel, the maximum pressure to be stored, and the strength properties of the material selected for fabrication of the inner matrix (maximum allowable stress). The material required to fabricate the outer surface has not been addressed in this comparison. Only the load bearing structures are being compared. The outer surface (of a pressure vessel which incorporates an inner matrix) is not a structurally critical part of the pressure vessel, and is does not represent a significant contribution towards total material. In fact, it may be fabricated of low cost, lightweight plastic.

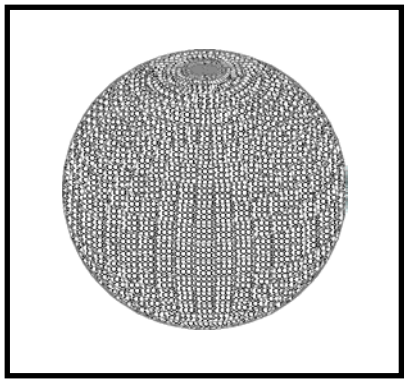

Figure 1.8: Spherical Inner Matrix

The volume of material required to fabricate the inner matrix is very simply the volume of the sphere ($v = 4\pi r^3 / 3$) times the relative density of the inner matrix structure (ρ). From Table 1.1, we see that in the case of a best case matrix, the required relative density is simply the pressure to be stored divided by the tensile strength of the parent material ($\rho_{relative} = P / \sigma_{material}$). This implies the required volume of structural material can

be expressed as: $V_{mtl} = 1.33\pi r^3 p/\sigma_{max}$. Again from Table 1, we see that in a poor case matrix expansion, the required relative density is much greater ($\rho_{relative} >> P/\sigma_{material}$).

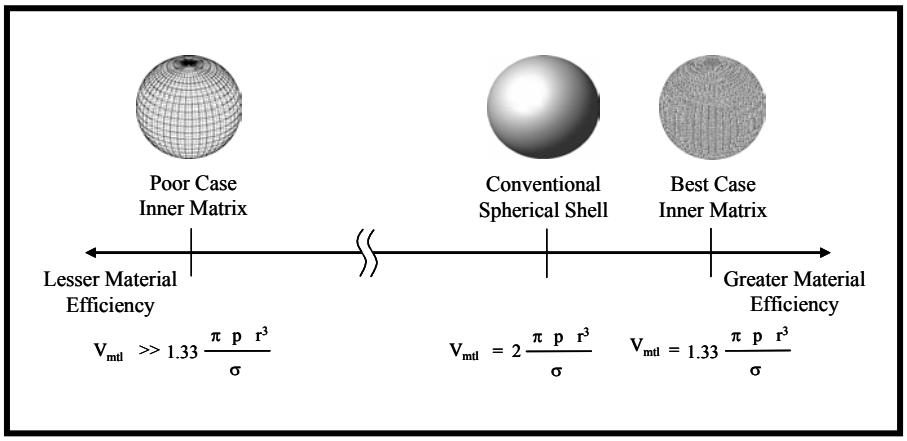

Figure 1.9: Comparison of various Inner Matrix types with a traditional Spherical Shell

By far, the vast majority of existing foams would produce Poor Case type Inner Matrices as shown above in Figure 1.9.

1.2.3 Cylindrical Shell Comparison

Again, a simple exercise reveals a relationship that describes the volume of structural material required to fabricate a conventional cylindrical pressure vessel that incorporates a traditional outer shell. The volume of structural material required is a function of the size (radius and length) of the pressure vessel, the maximum pressure to be stored, and the strength properties of the material selected for fabrication of the outer shell (maximum allowable stress).

Recall for thin walled cylindrical pressure vessels, Maximum Stress (Figure 1.10):

$$\sigma_{max} = \sigma_1 = pr/t$$

which can be restated in terms of required thickness as:

$$t = pr/\sigma_{max}$$

Where p = pressure, r = pressure vessel radius, and t = required wall thickness.

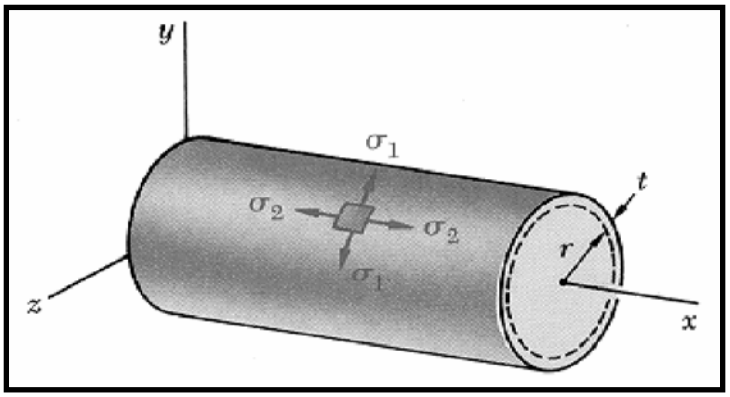

Figure 1.10: Thin Walled Cylindrical Shell

For a thin walled cylindrical pressure vessel, the volume of structural material required can be approximated by the product of the cylindrical surface area ($a = 2\pi rl$) times the wall thickness (t).

$$V_{mtl} = at = 2\pi rlt$$

Where V_{mtl} = volume of structural material, l = length, and a = surface area.

Which can be combined with the previous formula ($t = pr/\sigma_{max}$) to obtain:

$$V_{mtl} = 2\pi r^2 lp/\sigma_{max}$$

1.2.4 Cylindrical Inner Matrix

Again a simple exercise reveals a relationship that describes the volume of material required to fabricate a cylindrical pressure vessel that incorporates an inner matrix (Figure 1.11). Once more the volume of material required is a function of the size

(radius) of the pressure vessel, the maximum pressure to be stored, and the strength properties of the material selected for fabrication of the inner matrix (maximum allowable stress). The material required to fabricate the outer surface has not been addressed in this comparison. Only the load bearing structures are being compared. The outer surface (of a pressure vessel which incorporates an inner matrix) is not a structurally critical part of the pressure vessel, and is does not represent a significant contribution towards total material. In fact, it may be fabricated of low cost, lightweight plastic.

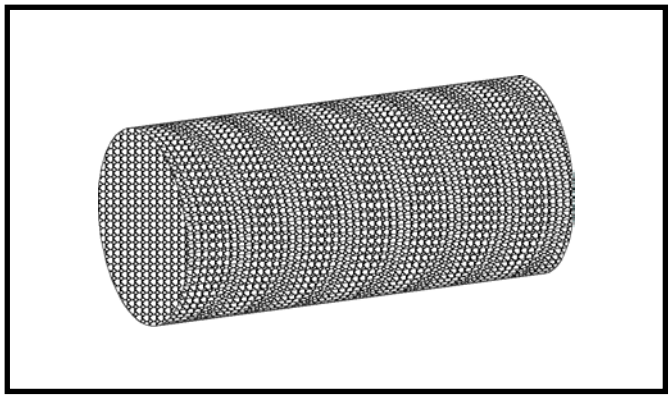

Figure 1.11: Cylindrical Inner Matrix

The volume of material required to fabricate the inner matrix is very simply the volume of the cylinder ($v = \pi r^2 l$) times the relative density of the inner matrix structure (ρ). From Table 1.1, we see that in the case of a best case matrix, the required relative density is simply the pressure to be stored divided by the tensile strength of the parent material ($\rho_{relative} = P / \sigma_{material}$). This implies the required volume of structural material can be expressed as: $V_{mtl} = \pi r^2 lp / \sigma_{max}$. Again from Table 1.1, we see that in a poor case matrix expansion, the required relative density is much greater ($\rho_{relative} >> P / \sigma_{material}$).

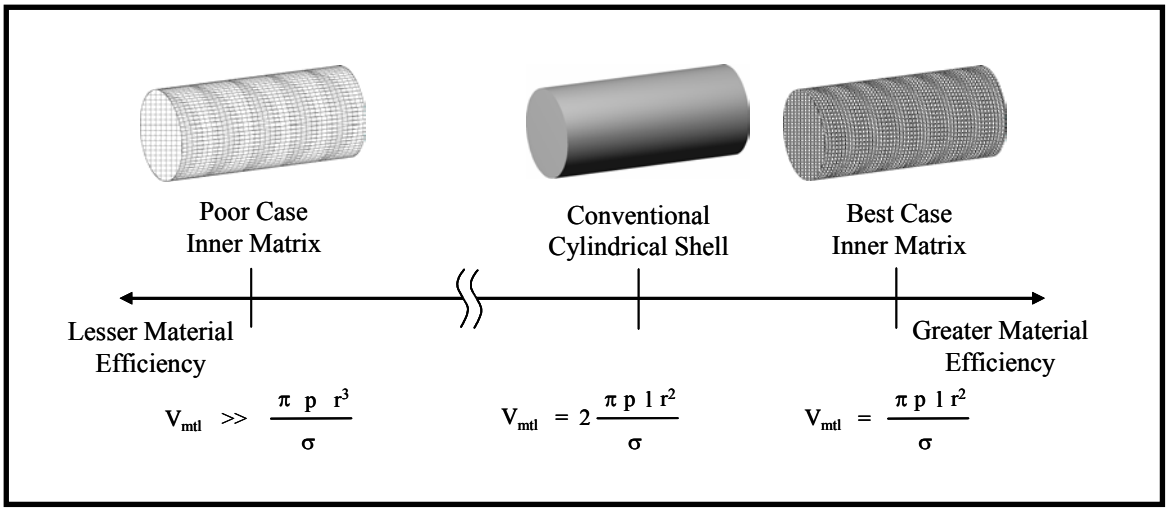

Figure 1.12: Comparison of various Inner Matrix types with a traditional Cylindrical Shell

By far, the vast majority of existing foams would produce Poor Case type Inner Matrices as shown above in Figure 1.12.

1.3 Hermetically Sealing Outer Surface Requirement

Use of an inner matrix to support a pressure vessel allows the use of a lighter weight thin outer surface. Unlike convention technology pressure vessels, the outer surface will not carry the structural loads. These structural loads will by definition be carried by the inner matrix. The outer surface must function as an impermeable membrane to contain the stored media (liquid and/or gas) under pressure within the physical boundaries of the inner matrix. This impermeable membrane will be connected to the inner matrix and contiguously supported over the entire outside surface of the pressure vessel by the inner matrix. Such an outer surface can be modeled as many small

circular shaped plates connected to each other and to the inner matrix on all their edges. Circles of widely varying radii will be present. The maximum radial size of these circles will be determined by the pore size of the inner matrix.

The outer surface thickness required for safe containment is a function of the maximum pressure to be stored, the maximum allowable stress for the selected outer surface material and the pore size of the inner matrix. This exercise will provide information concerning the minimum acceptable thickness for the outer surface of pressure vessels intended for low, medium and high pressure storage. The results will indicate that very thin outer surfaces will be all that is required for safe pressure retainment. In order to facilitate a rugged exterior that can weather abuse from external causes, a thicker than required outer surface should be considered. This will result in a product which a huge factor of safety with respect to the outer surface thickness.

In summary, because the outer surface will be connected to the inner matrix, a very thin outer surface is all that will be required for safe pressure retainment. However, a somewhat thicker than required outer surface should be considered for overall physical ruggedness. This will result in very safe pressure vessels.

1.4 Outer Surface Analysis Method

As stated earlier, the outer surface of an inner matrix supported pressure vessel can be modeled as many circular shaped plates. These circles will be of varying size with a maximum radius equal to the inner matrix pore radius. Roark's Formulas for Stress and

Strain provides a method for determining the maximum stress in polygon shaped plates with fixed edges. As it happens, the maximum stress develops in the middle of each straight edge. The information below is from case number 20 of table 26 in Roark's [3].

n	3	4	5	6	7	8	9	10	∞
β_2	1.423	1.232	1.132	1.068	1.023	0.99	0.964	0.944	0.75

$$\text{Max } \sigma = \frac{-\beta_2 \, q \, a^2}{t^2}$$

Where:

Max σ = Maximum Stress

β_2 = value from table above

a = Radius

q = Applied Pressure

t = Membrane Thickness

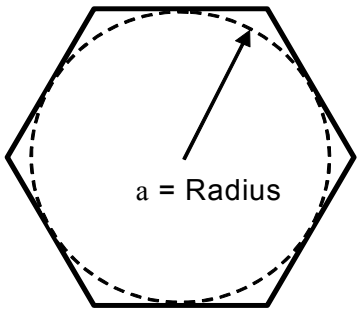

n = Number of sides

A circular plate is represented by the infinitely sided polygon and has a β_2 magnitude value equal to 0.75. We shall assume the radius, a equals a typical inner matrix pore radius of .0625 inches. This formula can be rewritten as shown for required outer surface thickness.

Where:

t = Required Membrane Thickness

β_2 = value from table above

a = Radius

q = Maximum Applied Pressure

Max σ = Maximum Allowable Stress

$$t^2 = \left| \frac{-\beta_2 \, q \, a^2}{\text{Max } \sigma} \right|$$

$$t = \sqrt{\left| \frac{-\beta_2 \, q \, a^2}{\text{Max } \sigma} \right|}$$

Use of a nearly ideal inner matrix which has a pore radius of 1/16th of an inch radius (8 pores per inch) shall be assumed for this example. A solid outer surface membrane of 6061 aluminum shall also be assumed. When properly tempered to a T6 condition 6061 aluminum exhibits a tensile yield strength of 40,000 psi. In order to solve for the worst case situation we shall solve for the maximum radii circular plates. Recall that:

$$t = \sqrt{\left| \frac{-\beta_2 \, q \, a^2}{\text{Max } \sigma} \right|}$$

Where:

t = Required Membrane Thickness

β_2 = 0.75 from Roark's table (∞ sides)

a = .0625 (1/16th inch)

q = 450 psi, 6,000 psi, 15,000 psi

Max σ = 40,000 psi

Parameter	Low Pressure	Med Pressure	High Pressure
Maximum Working Pressure	150	2,000	5,000
Burst Pressure (3 x Max Working Pressure)	450	6,000	15,000
Required Outer Surface Thickness (inches)	0.00597	0.02180	0.03447

These results help to further illustrate the superior efficiency of inner matrix supported pressure vessels. A solid outer surface of 6061 T6 Aluminum, 1/8th of an inch thick would be over three times thicker than required to safely (Factor of Safety = 3.0) contain 5,000 psi. Enormous factors of safety will result when reasonably thick outer surfaces are used. Clearly, a reasonably thick outer surface will never fail so long as the inner matrix remains intact.

CHAPTER 2. LITERATURE REVIEW

There is a long history of innovative and near innovative efforts to improve the performance and versatility of conventional spherical and cylindrical (outer shell type) pressure vessels. Most of these innovations involve the addition of supporting structural members to the outer shells. These innovations, representing the current state of the art, can be organized into those involving the addition of 1-dimensional axial supporting structural members, and those involving the addition of 2-dimensional planar supporting structural members.

2.1 1-Dimensional Solutions

One very illustrative example of the use of axial supports is the concept described in US patent number 4,840,282: Pressure-Resistant Tank [4]. Here the inventor has surrounded the exterior of a gang of partial cylindrical shells with an exoskeleton of sorts to achieve structural integrity. As shown in Figures 2.1, and 2.2 below, the exoskeleton system is composed of a plurality of axial support members.

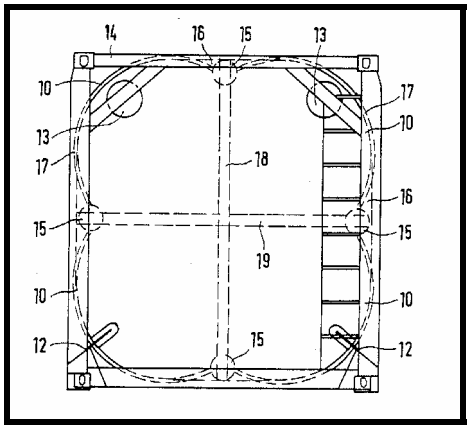

Figure 2.1: End View of the Exoskeleton System of Axial Supports [4]

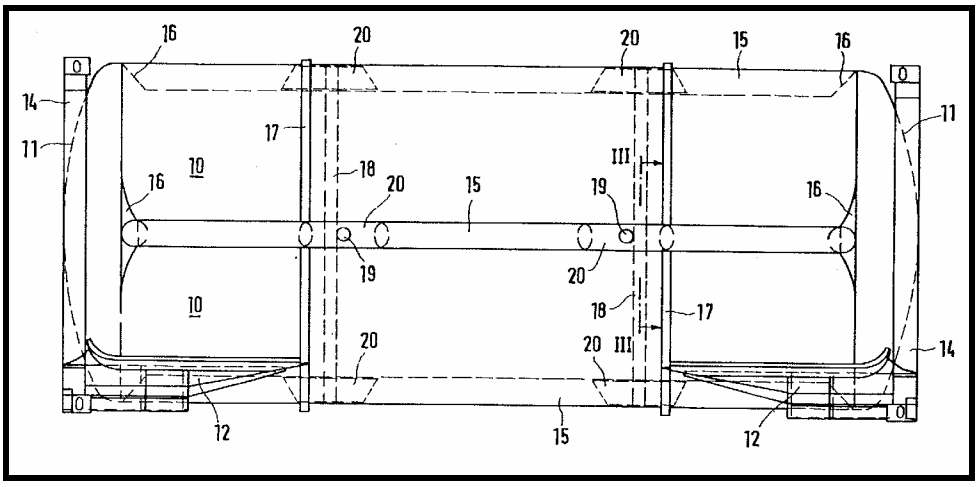

Figure 2.2: Side View of the Exoskeleton System of Axial Supports [4]

Another example of the use of axial support members to improve the performance and versatility of conventional outer shell type pressure vessels is US patent number 5,758,796: Pressure Vessel [5]. Here the inventor uses an internally mounted axial support member to improve the structural integrity of a cylindrical pressure vessel composed of three separate parts as shown below in Figures 2.3 and 2.4.

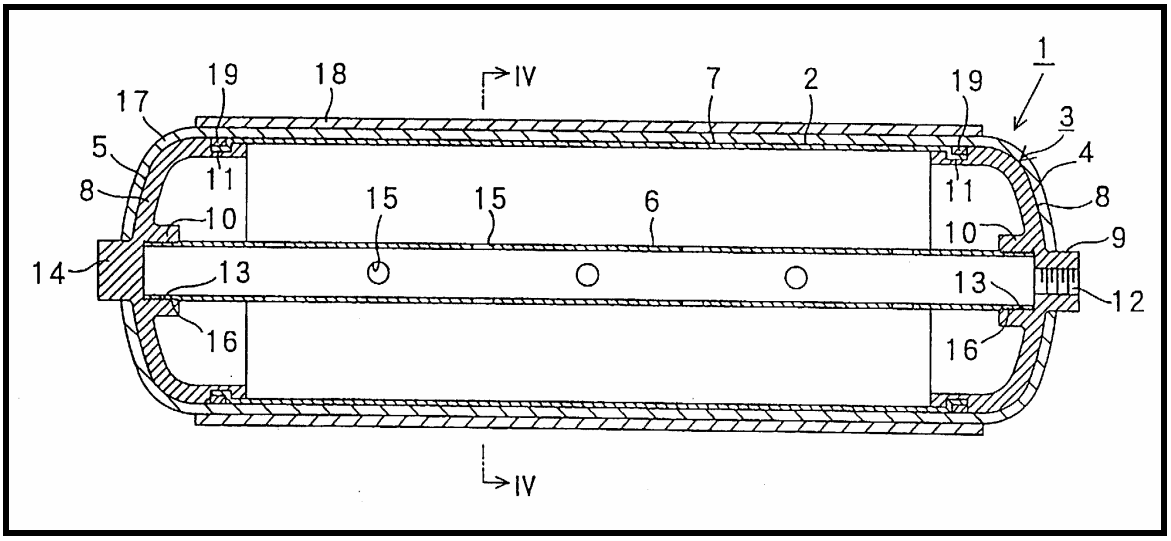

Figure 2.3: Internally Mounted Axial Support Member [5]

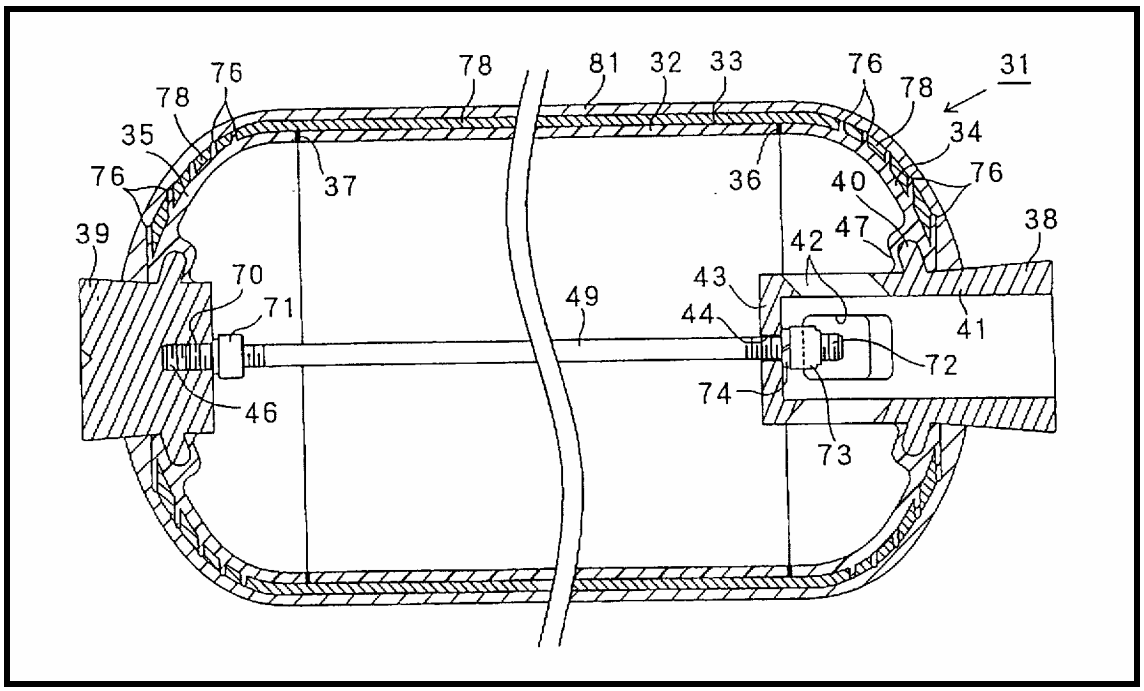

Figure 2.4: Internally Mounted Axial Support Member [5]

Another more innovative concept that reveals more 3-dimensional thinking than seen previously is the concept described in US patent number 5,462,193: Composite Pressure Vessel [6]. Here the inventor uses a multiplicity of internally mounted axial supports to achieve a fair degree of shape conformability. Though the effect on overall shape conformability may be 3-dimensional, the underlying method for achieving that objective involves the use of 1-dimensional axial supporting members. Figures 2.5 and 2.6 below illustrate this inventor's concept of using a multiplicity of 1-dimensional axial supports to achieve a 3-dimensional objective of shape conformability.

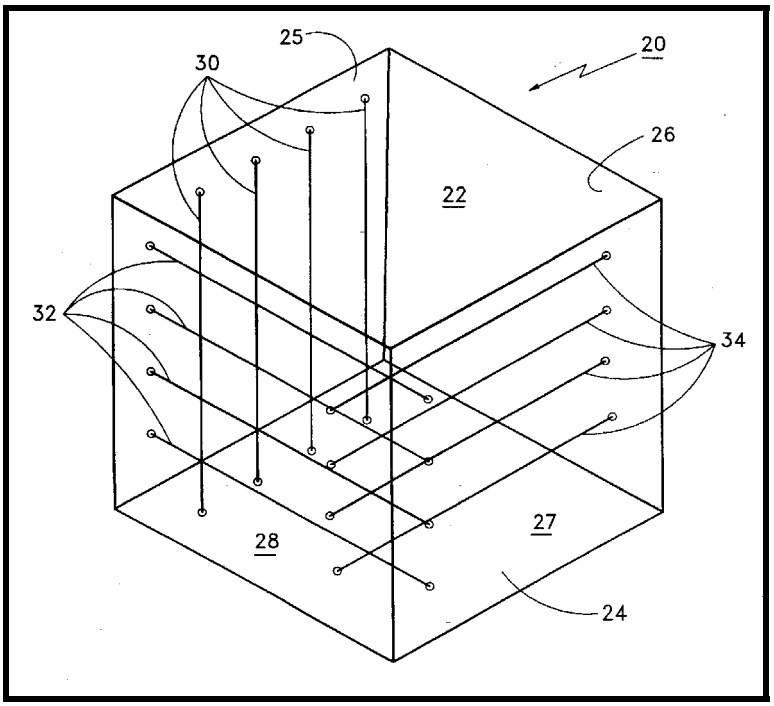

Figure 2.5: Multiplicity of 1-Dimensional Axial Supports [6]

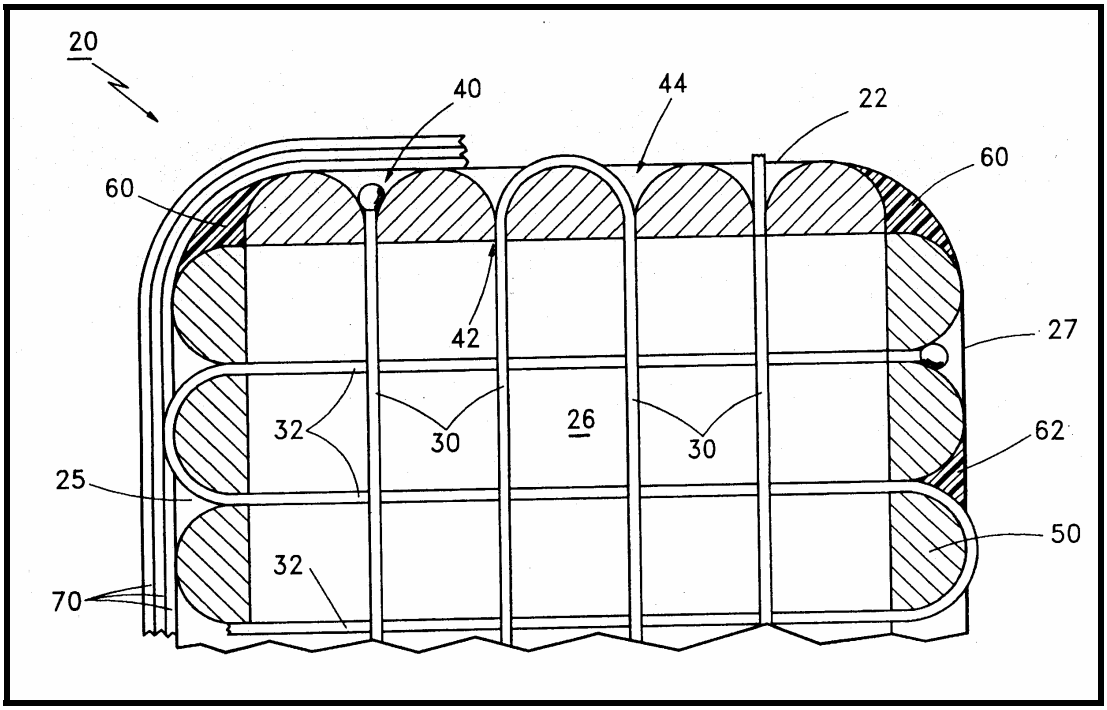

Figure 2.6: Outer Surface Detail [6]

Another example that seems highly inspired by the previous example is US patent number 5,647,503: Tank For Storing Pressurized Gas [7]. This example is included primarily because the illustrations (Figures 2.7 and 2.8) are a bit more revealing, and the previous example is included because it seems to be the parent concept.

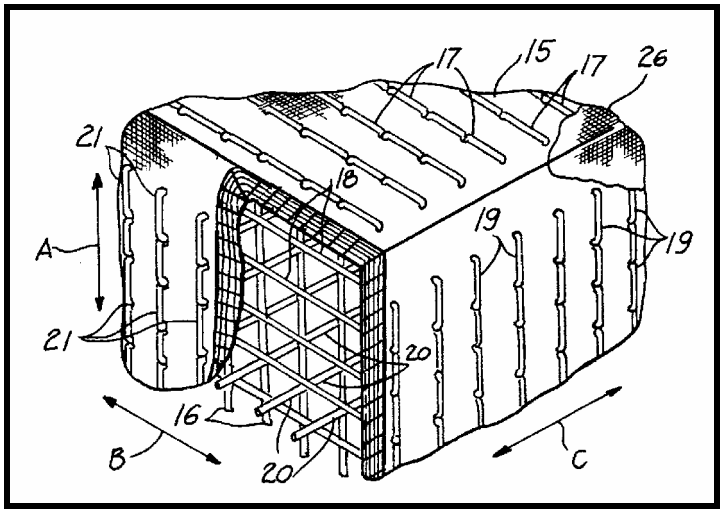

Figure 2.7: Multiplicity of 1-Dimensional Axial Supports Again [7]

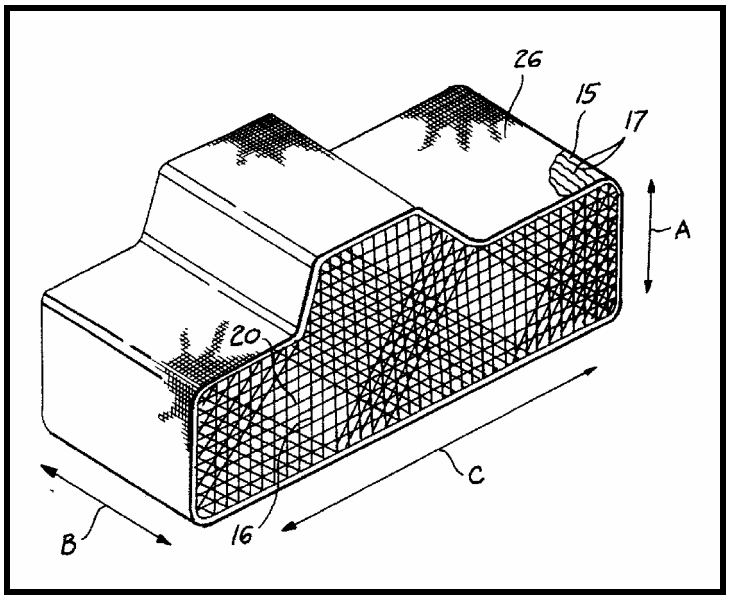

Figure 2.8: 3-Dimensional Result [7]

The final example involving the use of 1-dimensional axial supports to improve the performance and versatility of pressure vessels is the use of open cell aluminum foam as an internally mounted structural support as described in the unpatented but published work of ERG Aerospace, Inc [8]. While the open cell support structure is obviously 3-dimensional, it is functionally composed of a multiplicity of connected axial supports. See Figures 2.9 and 2.10 below.

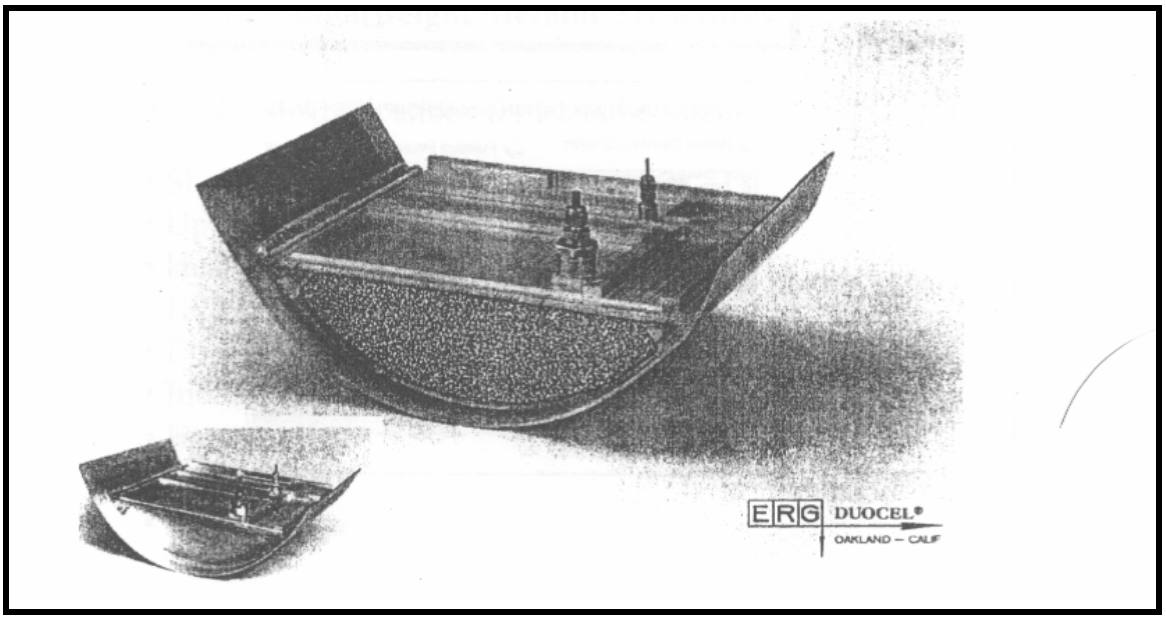

Figure 2.9: Open Cell aluminum Foam as an Internally Mounted Structural Support [8]

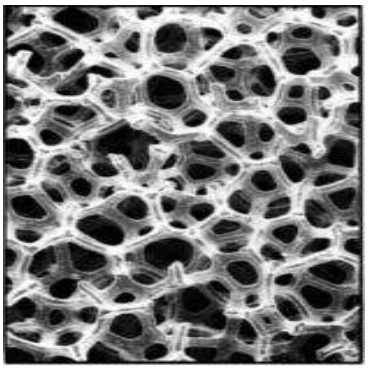

Figure 2.10: Open Cell Foam is a Multiplicity of Connected Axial Supports [8]

2.2 2-Dimensional Solutions

The next set of examples (Figures 2.11 and 2.12) involves the use of 2-dimensional planar support structures to improve the performance and versatility of conventional spherical and cylindrical outer shell pressure vessels. The use of planar support structures represents an improvement over the use of axial support structures from a structural efficiency standpoint.

The first example involves the use of radially symmetrical planar support structures inside a conventional cylindrical pressure vessel as described in US patent number 5,564,587: Pressure Container [9]. Here the inventor incorporates the planar supports along with the outer shell as one monolithic structure connected to attachable end caps.

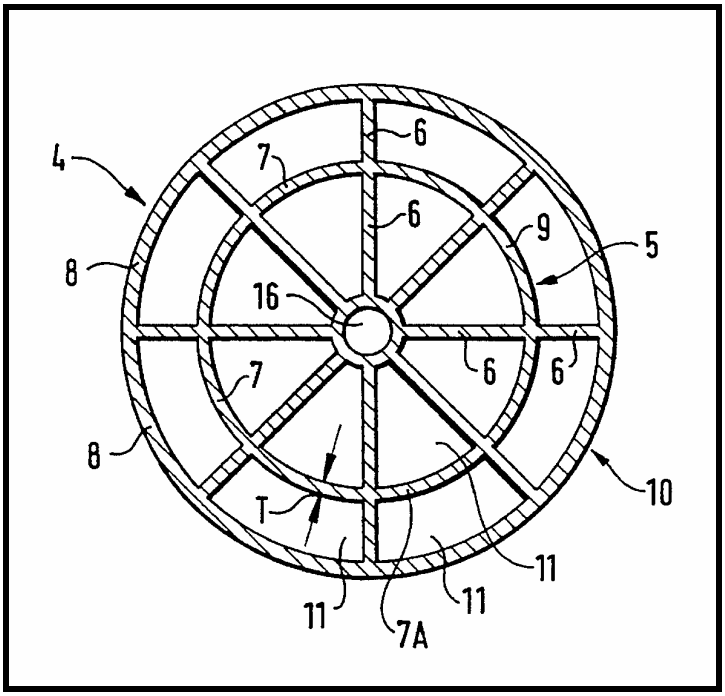

Figure 2.11: Radially Symmetrical Planar Support Structures [9]

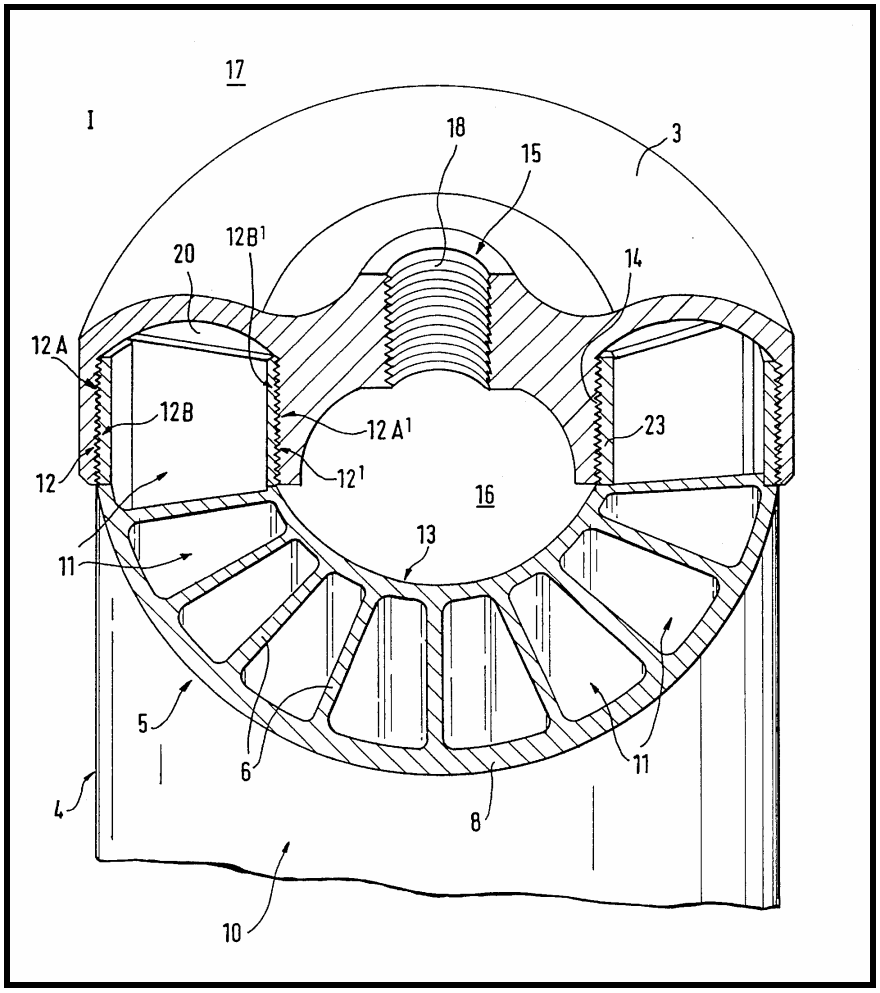

Figure 2.12: One Monolithic Structure Connected to Removable End Caps [9]

The next example involves the use of planar support structures mounted inside the pressure vessel to allow for limited conformal shaping of the vessel. US patent number 5,323,953: Pressurized Storage For Gases [10]. Figure 2.13 illustrates this use of 2-dimensional supports to achieve 3-dimensional results. The contiguously supported internal planar structures include small passages to allow the stored media to easily migrate the entire interior of the vessel as shown in Figure 2.14 below.

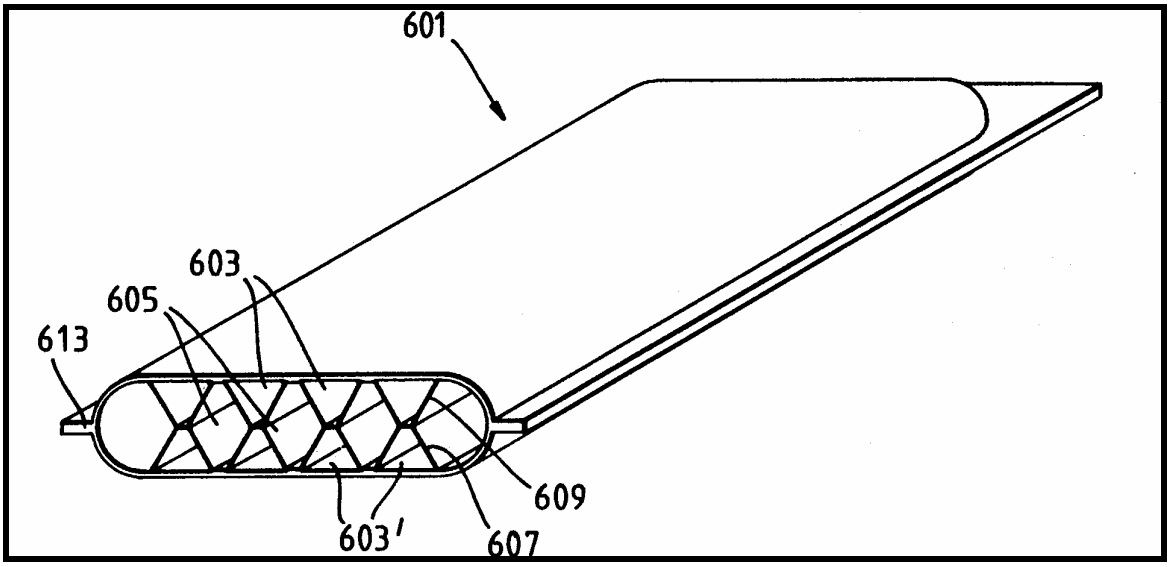

Figure 2.13: 2-Dimensional Supports Achieve 3-Dimensional Results [10]

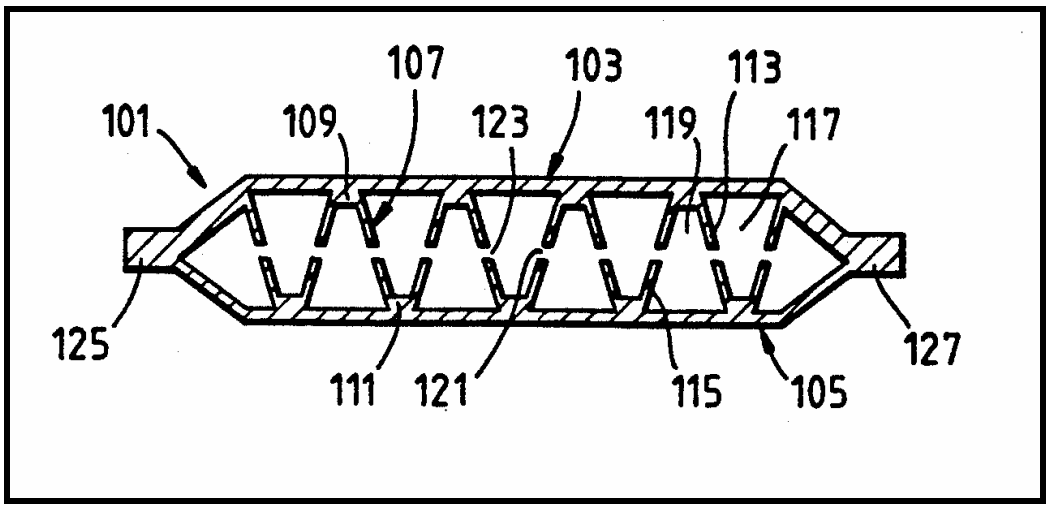

Figure 2.14: Small Passages to Allow the Stored Media to Easily Migrate [10]

The invention disclosed in US patent number 4,946,056: Fabricated Pressure Vessel [11], illustrates the use of internally mounted planar support structures to facilitate the combining of multiple cylindrical segments into a single structure (see Figure 2.15),

allowing for the more efficient use of non-cylindrical special envelops. This method also involves the use of small passages to facilitate the easy migration of the stored media as shown in Figure 2.16 below.

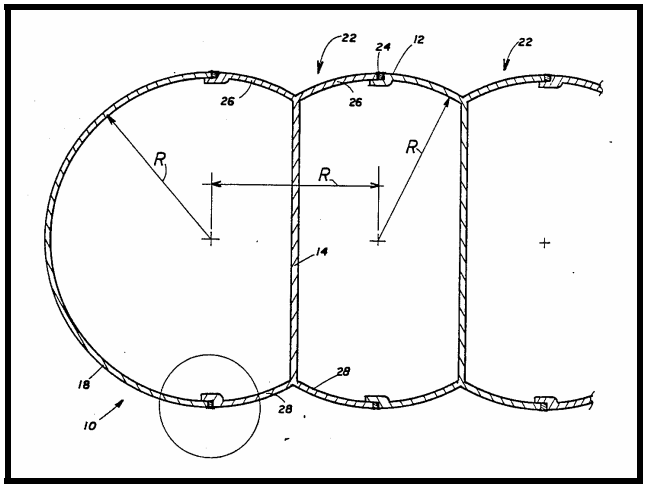

Figure 2.15: Planar Support Structures Facilitate the Combining of Multiple Cylindrical Segments [11]

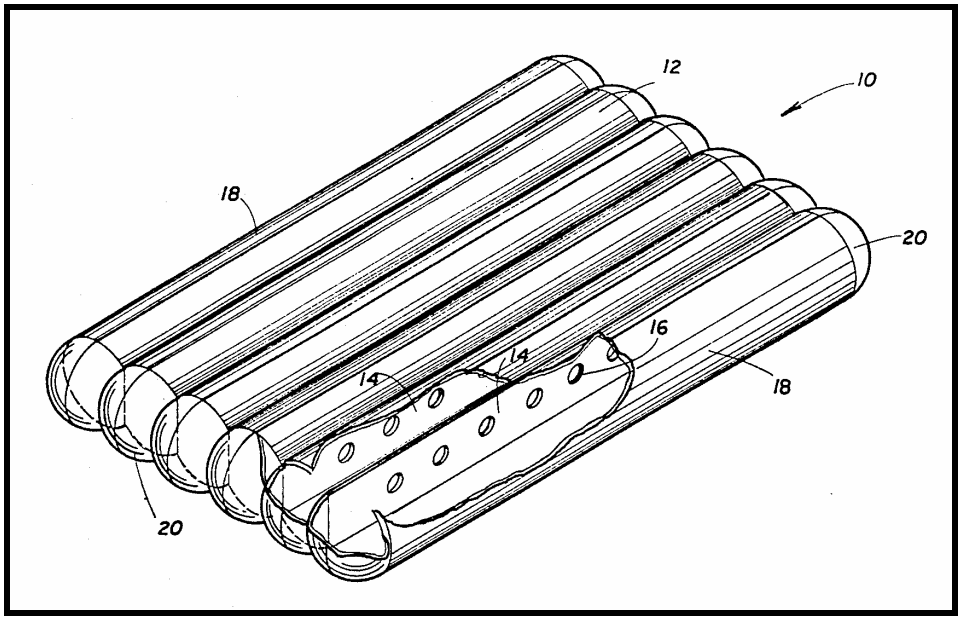

Figure 2.16: Small Passages Facilitate the Easy Migration of the Stored Media [11]

Lastly, we examine US patent number 5,577,630: Composite Conformable Pressure Vessel [12]. This invention seems to be largely inspired by the disclosures in the previous patent (see Figure 2.17 below). However, as shown in Figure 2.18, this patent adds some extra details related to the use of composite materials for fabrication.

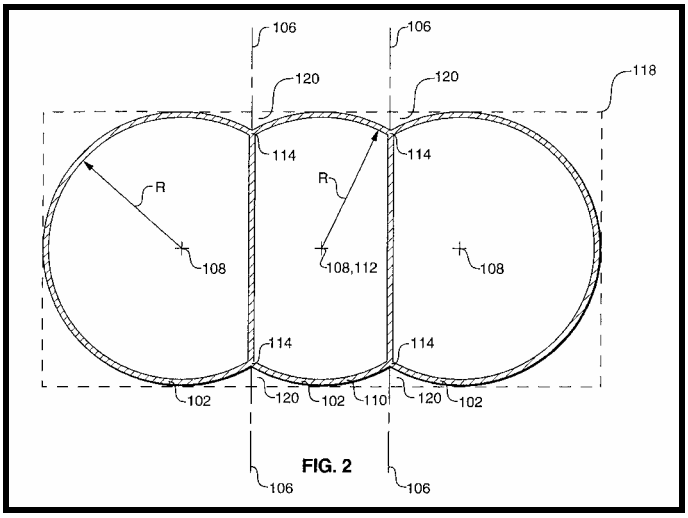

Figure 2.17: Planar Support Structures Facilitate the Combining of Multiple Cylindrical Segments [12]

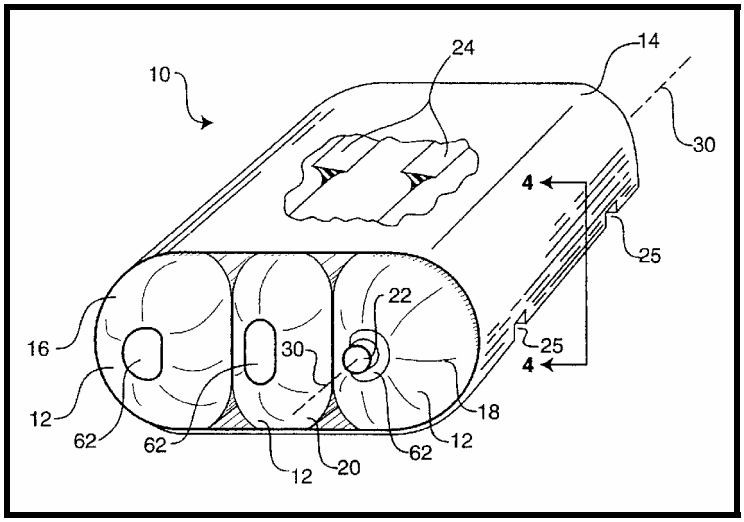

Figure 2.18: This Patent Adds Some Extra Details Related to the Use of Composite Materials [12]

2.3 Summary

As a whole group, the pressure vessels described above, representing the current state of the art, by incorporating 1-dimensional axial support structures, and/or 2-dimensional planar support structures, do make some progress in achieving the goal of increasing the versatility of the designs by allowing for non-spherical and non-cylindrical shapes. But, they are all far more massive and far more difficult to manufacture than their conventional spherical or cylindrical outer shell counterparts. These negative characteristics have resulted in a lack of wide-scale interest and development. As described in the following chapters, these short comings are effectively addressed and remedied through the use of a 3-dimensional triaxial support structure called an HPR^{TM} inner matrix.

CHAPTER 3. INDUSTRY SURVEY

Due to the special material properties of metal, selection of metal foam offers the most obvious solution for an HPR™ inner matrix material. However, metal foam fabrication is a relatively new technical area. Several different approaches to the fabrication of metal foam have been developed, each offering different results [1]. From an HPR™ inner matrix perspective, some metal foam fabrication techniques seem superior to others.

3.1 Overview

Foam microstructure plays a very critical role in determining if the foam might be useful as an HPR™ inner matrix in a Pressure Vessel. In summary, an ideal HPR™ inner matrix in a pressure vessel has all of its structural material subjected to omni-directional tri-axial (hydrostatic) tension when pressure is applied to the vessel. While the best case condition can get no better than this ideal situation, a less than best case condition can get much worse. In fact, the foamed material can arrange itself with many folds and zigzags that tend to cause some portion of the material to be in a position to provide no support at all. This is exactly what happens with many if not most metal foams. Figure 3.1 illustrates this effect as a variety of foams are compared for relative strength (strength of the foamed material/strength of a solid block of the same material) as a function of relative density (density of the foamed material/density of a solid block of the same material). For clarity a line has been added to represent the ideal HPR™ situation where all the material is loaded in a tri-axial state, and another line to represent

the attainment of 80% of the ideal condition. Data for a polymeric foam produced by DIAB has also been added as an example of the practical levels of performance that have already been attained in the real world.

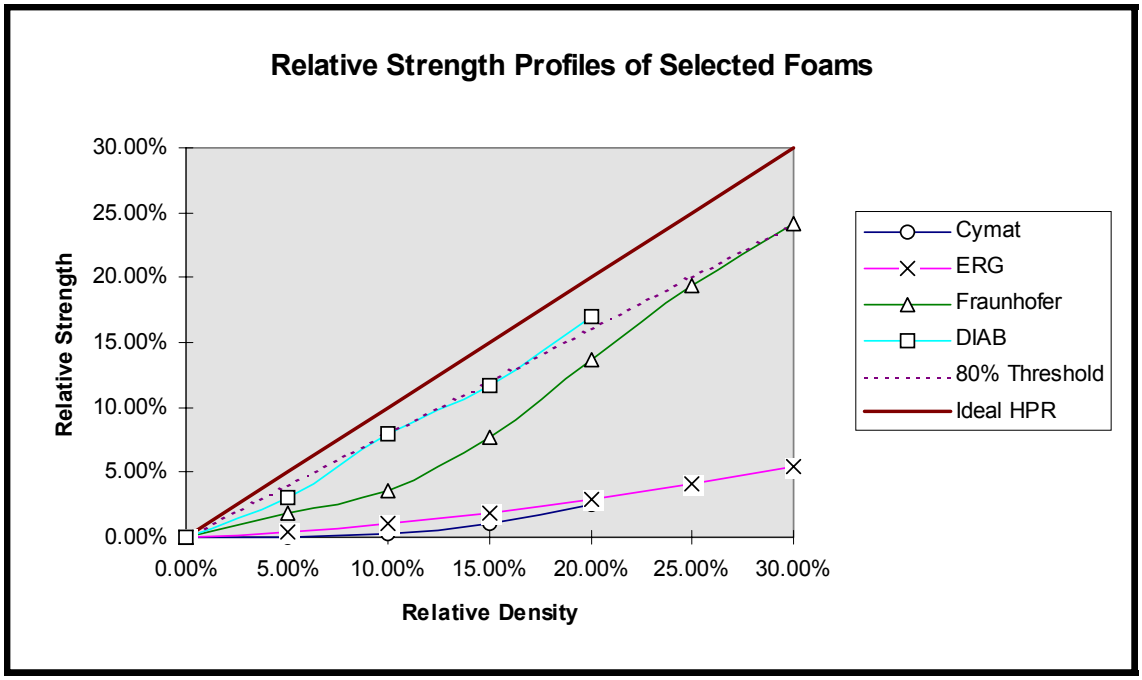

Figure 3.1: Relative Strength Profiles

Obviously, all foams are not equal when it comes to strength retention. Since, the results in Figure 3.1 are each normalized for reference against solid blocks of the same material, the differences are assumed to be caused by the different microstructures of the various foams. Evidently, some microstructure is measurably superior to the others for strength retention. It appears, one very best pattern of bubble shaping, distribution, and spacing (superior microstructure) which yields the greatest level of strength retention, especially at lower relative densities. This one very best pattern of bubble shaping, distribution, and spacing represents the “Holy Grail” of foam microstructures -- because

generally, foam (open-cell foam in particular) makes a poor choice as structural support inside pressure vessels. That is of course, unless the foam has this very special microstructure (or something very close) which supports a high level of strength retention via maximized material loaded in a tri-axial state, or HPR^{TM}. Based on the results of this survey, this very special microstructure seems to be one where all of the bubbles are: substantially spherical in shape, substantially the same size (no extra-large bubbles), and scattered in a substantially homogeneous distribution. In addition, the holes which connect the bubbles must be very small in comparison to the bubble diameter.

3.2 Cymat Foam

The data for Cymat's foam came from information provided by Cymat Aluminum Foam Corporation [13]. Cymat produces a closed cell aluminum foam using a direct foaming process patented by and licensed from Alcon. Their process involves injecting gas bubbles into molten aluminum and skimming the foam off the top (see Figure 3.2).

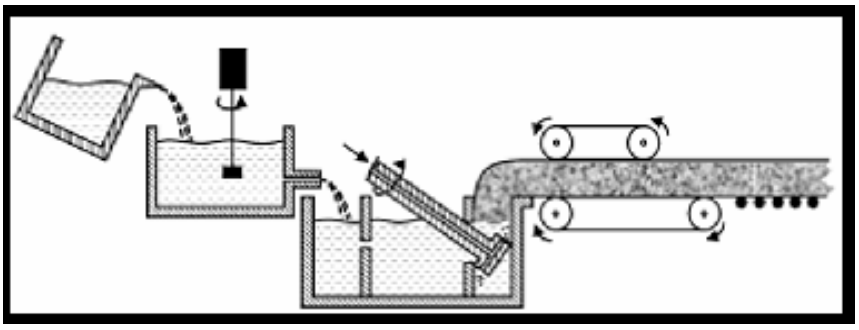

Figure 3.2: Cymat Foaming Process [1]

The process results in a very low cost product {sale price of about $5.00 USD per pound (about $84 USD per cubic foot for 10% foam)}, which exhibits very little retention of its potential strength. For this reason, the Cymat closed cell aluminum foam product would

be a poor choice for a structural support inside a pressure vessel. Figure 3.3 below shows the Cymat foam microstructure.

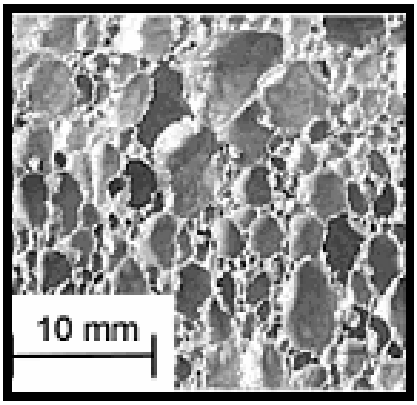

Figure 3.3: Cymat Foam Microstructure [1]

3.3 ERG Foam

The data for ERG's foam is provided by ERG Materials and Aerospace Corporation [14]. The relation for relative strength as a function of relative density is expressed as:

$$\sigma_{foam}/\sigma_{solid} = .33(\rho_{foam}/\rho_{solid})^{3/2}$$

This formula for Relative Strength is an approximation which is characteristic of all open cell foams due to the similarity of their physical structures (interior morphologies). ERG produces open cell aluminum foam using an investment casting process (see Figure 3.4 below). This results in a very expensive product {sale price of about $1.00 USD per cubic inch ($1,728 USD per cubic foot) plus labor for the additional efforts}, which exhibits very little retention of its potential strength. In addition, ERG will not sell raw foam. They will only sell finished products which utilize their foam (hence, the additional efforts and the related costs which normally amount to much more than the

cost of the foam). The EGR open cell aluminum foam product would also be a poor choice for a structural support inside a pressure vessel. Figure 3.5 below shows the ERG foam microstructure.

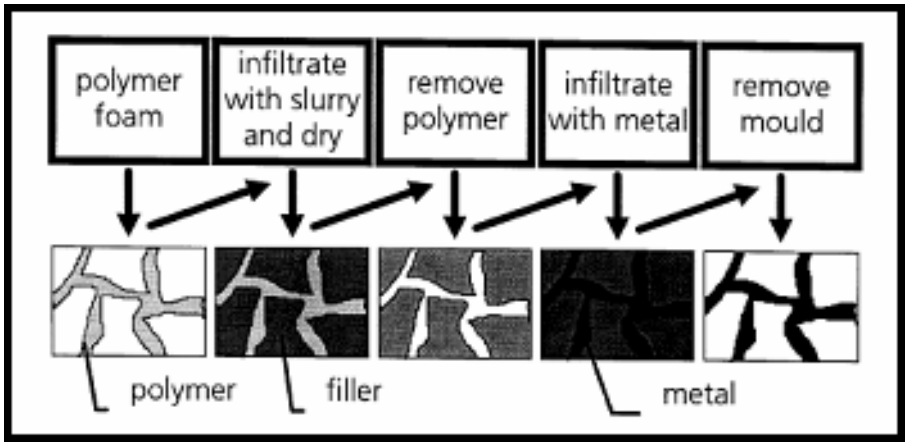

Figure 3.4: ERG Foaming Process [1]

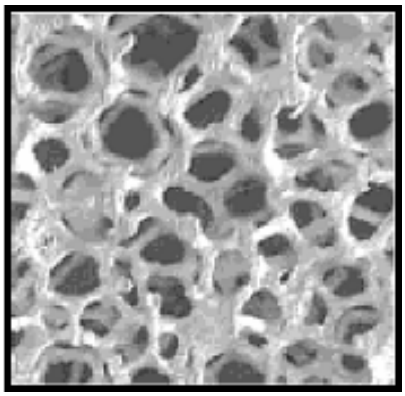

Figure 3.5: ERG Foam Microstructure [1]

Note: ERG has in the past used their foam as a structural support inside of irregularly shaped pressure vessels. For a nice cut-away view of one of these products, please see Figure 2.9 in Chapter 2. Clearly, as illustrated in Figure 3.5 above, the ERG open cell foam is not an efficient structural support. These pressure vessels are also very

expensive, costing several tens of thousands of dollars each (several $10,000 USD each). Without the special additional requirements for heat exchange and slosh baffling, this approach is neither cost nor structurally effective. While the cost effectiveness is a function of ERG pricing, the structural effectiveness is a function of the physical/structural properties of open cell foam.

3.4 Fraunhofer Foam

The data for Fraunhofer comes from a presentation made by J. Banhart & J. Baumeister entitled 'Deformation Characteristics of Metal Foams' [15]. Additional information used for normalization was provided by the Fraunhofer Resource Center in Delaware. Fraunhofer uses their patented powder metallurgical method (see Figure 3.6 below). The process results in a very reasonable cost product (sale price of about $100 - $200 USD per cubic foot), which exhibits a reasonable retention of its potential strength. In addition, the Fraunhofer process stands alone from the others due to its ability to produce complex 3-dimensional shaped configurations which also have a nearly impermeable dense outer surface covering. However, the Fraunhofer process must be modified to produce small perforations through the cell walls of the closed cell foam. The Fraunhofer closed cell aluminum foam product as modified to produce small perforations between the cells is a reasonable choice for a structural support inside a pressure vessel. Figure 3.7 below shows the Fraunhofer foam microstructure.

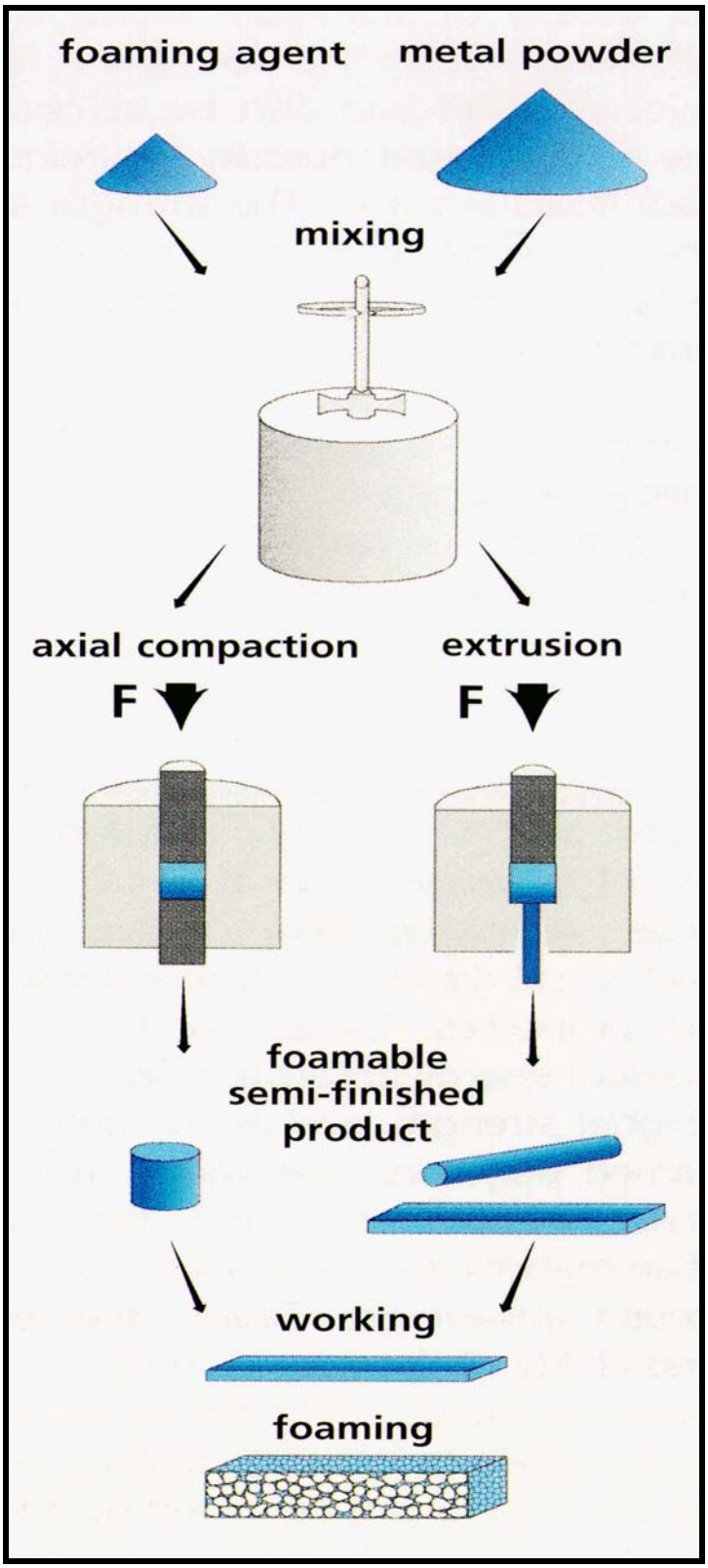

Figure 3.6: Fraunhofer Foaming Process [1]

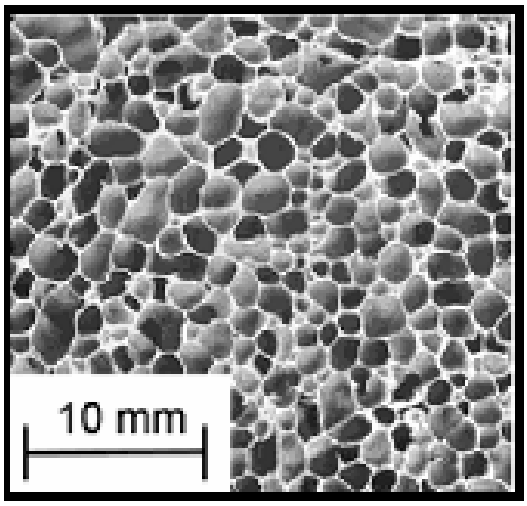

Figure 37: Fraunhofer Foam Microstructure [1]

3.5 DIAB Foam

The data for DIAB was provided by Divinycell International AB [16]. The DIAB product is a polymeric foam which exhibits the greatest retention of its potential strength of any foam product identified in the survey. Therefore, the DIAB foam (Divinycell H) is an example of what is attainable in the real world. Notice, the DIAB foam suggests an overall ability to retain about 80% of its potential strength (as defined by an ideal structure which has all of its material loaded in a tri-axial state). This 80% guideline seems valid to Relative Densities as low as 10%. At Relative Densities lower than 10%, it seems that real world limitations cause the foam to retain lesser amounts of its potential strength (probably due to the development of irregular shaped and extra-large bubbles at very low relative densities). Note: It must be recognized that unreinforced polymeric materials are not compatible for use on pressure vessels due to creep, and that HPR^{TM} is most useful with homogeneous isotropic materials (not composites). Therefore, the DIAB foam data is presented as an example of a nearly ideal HPR^{TM} morphology, not as

a candidate structural material. Figure 3.8 shows the very high quality DIAB foam microstructure.

Figure 3.8: DIAB Foam Microstructure

3.6 Review

A weight savings projection of 33% for spheres and 50% for cylinders is based on an ideal situation (not real world) with an inner matrix inside an HPR^{TM} pressure vessel comprised of superior foam exhibiting the characteristic of all of the material loaded in a triaxial state, or ideal HPR^{TM}. As demonstrated herein, it is possible to attain 80% of this idea situation by ensuring the foam has a special microstructure. The Fraunhofer foam is better than all the other metal foams in this respect, but it is not as good as the DIAB polymeric foam. This indicates there is room for improving the microstructure of the Fraunhofer foam.

In order to get a more useful and detailed look at what is happening in Figure 3.9, each of the Relative Strength data points are divided by the corresponding ideal HPR™ Relative Strengths. This yields data which represents a percentage of the total potential strength achieved as a function of Relative Density. For example, at a Relative Density of 15%, the Cymat foam exhibits a Relative Strength of 1.03%. A foam with ideal HPR™ characteristics would exhibit a Relative Strength of 15% because all of the material would be loaded in a triaxial state. Therefore, the Cymat foam (due to imperfections in its microstructure) attains only 1.03/15 = 6.87% of its potential. This new foam characteristic is defined as the HPR™ Efficiency. The Cymat foam exhibits an HPR™ Efficiency of 6.87% at a Relative Density of 15%. Figure 3.9 below illustrates the HPR™ Efficiencies of the same set of selected foams shown in Figure 3.1. The DIAB polymeric foam demonstrates a real world HPR™ Efficiency near or above 80% for all Relative Densities above 10%. The Fraunhofer metal foam with its current morphology, demonstrates a real world HPR™ Efficiency of about 40% at 10% Relative Density. The HPR™ Efficiency of the Fraunhofer foam gradually improves with increasing Relative Densities until it attains the 80% threshold at a Relative Density of about 30%. It can be reasonably assumed that these HPR™ Efficiencies will all improve with increasing Relative Densities. However, our application is probably best served by foams with Relative Densities of 30% or less.

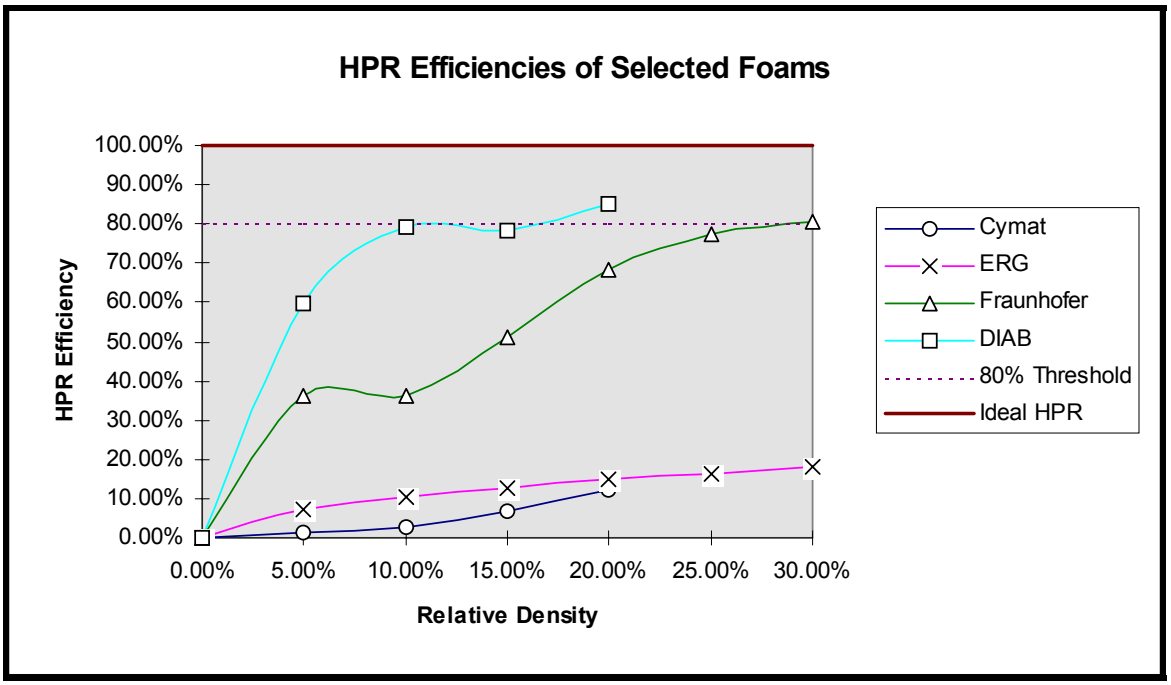

Figure 3.9: HPR^{TM} Efficiencies

Based on the results of this survey, there seems to be a practical limit of 80% on HPR^{TM} Efficiency depending upon Relative Density. Applying the 80% figure to the previously derived volumetric ratios, allows for a reasonable estimate of the practical weight saving potential of HPR^{TM} pressure vessels. Recall for a conventional spherical shell pressure vessel that the volume of structural material required can be expressed as: $V_{mtl} = 2\pi r^3 p/\sigma_{max}$, and that for an ideal spherical HPR^{TM} pressure vessel the volume of structural material required can be expressed as: $V_{mtl} = 1.33\pi r^3 p/\sigma_{max}$. This implies a practical weight saving of: (2.00 – (1.33/0.80)) / 2.00 = 16.7% for spherical pressure vessels. Further recall, for a conventional cylindrical shell pressure vessel that the volume of structural material required can be expressed as: $V_{mtl} = 2\pi r^2 lp/\sigma_{max}$, and that for an ideal cylindrical HPR^{TM} pressure vessel the volume of structural material required

can be expressed as: $V_{mtl} = \pi r^2 lp/\sigma_{max}$. This implies a practical weight saving of: (2.00 – (1.00/0.80)) / 2.00 = 37.5% for cylindrical pressure vessels.

It should be noted that these weight saving estimates are conservative. In both cases, the conventional sphere and conventional cylinder would each need to be increased in size a bit to hold the exact same quantity of gas as the equivalent HPR^{TM} vessels. This is because they each have more structural material taking up space inside the equivalent (same outside diameter) envelopes. This is one among many counter-intuitive aspects of HPR^{TM}. Let's assume the extra weight is used to account for a thin outer shell over each HPR^{TM} matrix.

3.7 Summary

In summary, HPR^{TM} pressure vessels can be reasonably expected to perform very well when compared to conventional spherical shell pressure vessels in material efficiency. Use of an ideal inner matrix can theoretically yield a 33% improvement in strength. A 16.7% improvement represents a practical goal when compared to spheres. When comparing to conventional cylindrical shell pressure vessels, use of an ideal inner matrix can theoretically yield a 50% improvement in strengthi. A 37% improvement represents a practical goal when compared to cylinders.

Therefore, in a head-to-head comparison with all other parameters left equal; same size and shape, same pressures, same materials, same maximum allowable stresses (factors of safety), HPR^{TM} technology shows itself to be potentially superior to

conventional technology in material efficiency. Therefore HPR™ pressure vessels fabricated in any shape may weigh less and potentially even cost less than conventional counterparts.

Add to this advantage the fact that HPR™ pressure vessels can be fabricated into any conceivable shape with no compromise in strength, weight, safety or cost. In addition, HPR™ technology provides enhanced safety features. Plus, the load carrying structure is safely protected inside the pressure vessel rather than exposed to the outside world.

CHAPTER 4. THEORY

Investigation reveals that the inner matrix microstructure (Figure 4.1) effects HPR^{TM} efficiency. The key variable parameters that determine the quality of the inner matrix microstructure from an HPR^{TM} efficiency perspective areas follows; bubble shape distribution/homogeneity, bubble size distribution/homogeneity, bubble position (packing structure) distribution/homogeneity, and bubble spacing distribution/homogeneity. By definition, HPR^{TM} is based on maximizing the occurrence of tri-axial tension in the structural material. Generally, this requires symmetry and homogeneity to be preferred characteristics of an inner matrix microstructure. So, for the purposes of this analysis, spherical bubbles of a single size shall be assumed for reasons of symmetry and homogeneity. However, the existence of a favored bubble packing structure or favored bubble spacing arrangement is not immediately apparent. A closer examination of these parameters follows.

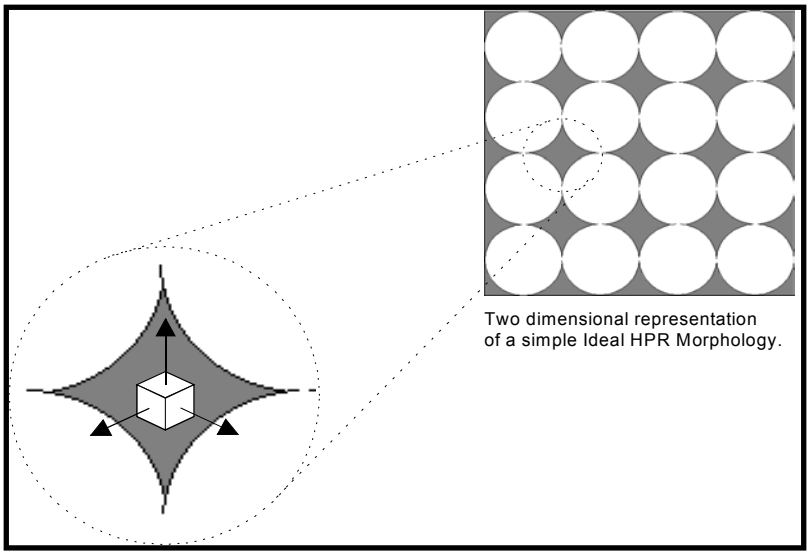

Figure 4.1: Inner Matrix Microstructure

4.1 Bubble Packing Structures

There are three basic bubble packing structures suitable for investigation. Each bubble packing structure exhibits optimized symmetry and homogeneity. They differ only in packing efficiency. They are simple cubic, body centered cubic, and face centered cubic. The simple cubic packing structure is most easily described by starting with a unit cube of structural material and positioning the one bubble at each corner as shown below in Figure 4.2. The packing efficiency for the simple cubic packing structure achieved when the bubble surfaces just touch each other is 0.523599 or approximately 52% [17].

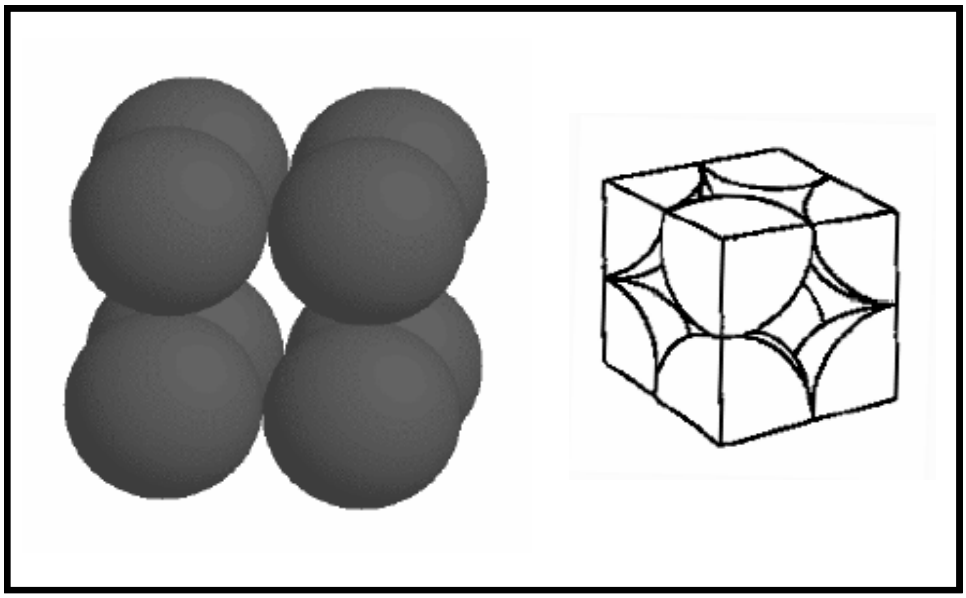

Figure 4.2: Simple Cubic Packing Structure

The body centered cubic packing structure is most easily described by starting with a unit cube of structural material and positioning the one bubble at the center and

then positioning one bubble at each corner as shown below in Figure 4.3. The packing efficiency for the body centered cubic packing structure achieved when the bubble surfaces just touch each other is 0.680175 or approximately 68% [17].

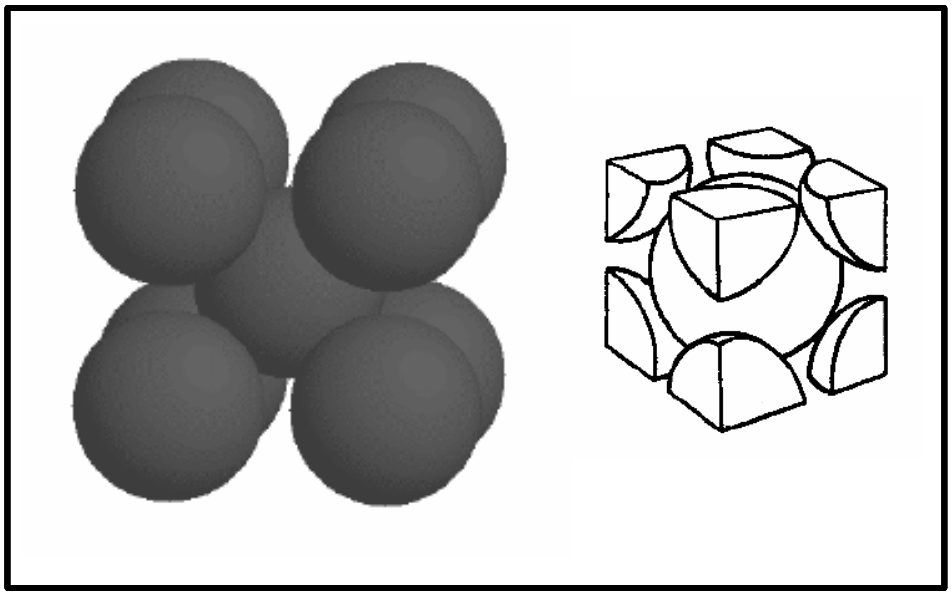

Figure 4.3: Body Centered Cubic Packing Structure

The face centered cubic packing structure is most easily described by starting with a unit cube of structural material and positioning the one bubble at the center of each face and then positioning one bubble at each corner as shown below in Figure 4.4. (Note: This pattern of spherical bubble packing is quite similar to, but subtly different from the hexagonal-close-packed packing structure, which has the exact same packing efficiency.) The packing efficiency for the face centered cubic packing structure achieved when the bubble surfaces just touch each other is 0.740480 or approximately 74% [17]. Johannes Kepler determined in 1611 that the densest packing of spheres in space is accomplished with the face centered cubic arrangement. Since he offered no proof of this assertion, it

has become known as the Kepler Conjecture [18]. Recently, however, Thomas C. Hales, Professor of Mathematics at the University of Pittsburg, has offered a proof of the Kepler Conjecture [19]. Since Hales' proof is some 250 pages long, and includes gigabytes of computer files, final verification may take awhile. Regardless of any final verification of Dr. Hales' impressive and long awaited (400 years) proof, the Kepler Conjecture is good enough for this researcher. The face centered cubic bubble packing structure shall be assumed to be the ideal packing structure for HPR™ inner matrices.

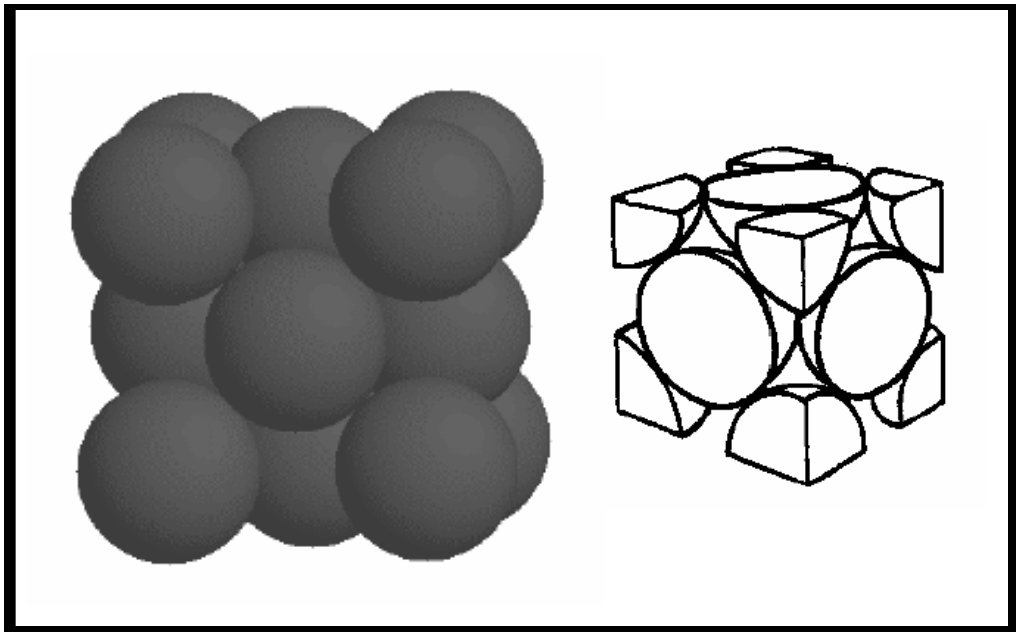

Figure 4.4: Face Centered Cubic Packing Structure

4.2 Bubble Spacing Effects

Bubble spacing is also of great importance in determining HPR™ efficiency. As shown in Figure 4.5 below, HPR™ inner matrices, which rely upon maximizing the

quantity of structural material subjected to triaxial tension, must have a microstructure that maximizes the quantity of structural material with all three axes unencumbered, even if by a circuitous path. Notice in Figure 4.5, a bubble can only get so close before it begins to interfere with unencumbered triaxial tension. The obstruction to triaxial tension caused by bubble proximity results in a zone, or layer of angular distortion near the surface of the bubble. Due to the effect of induced shear stresses, the maximum total stress within this angular distortion zone will be far greater than the maximum total stress outside of the zone.

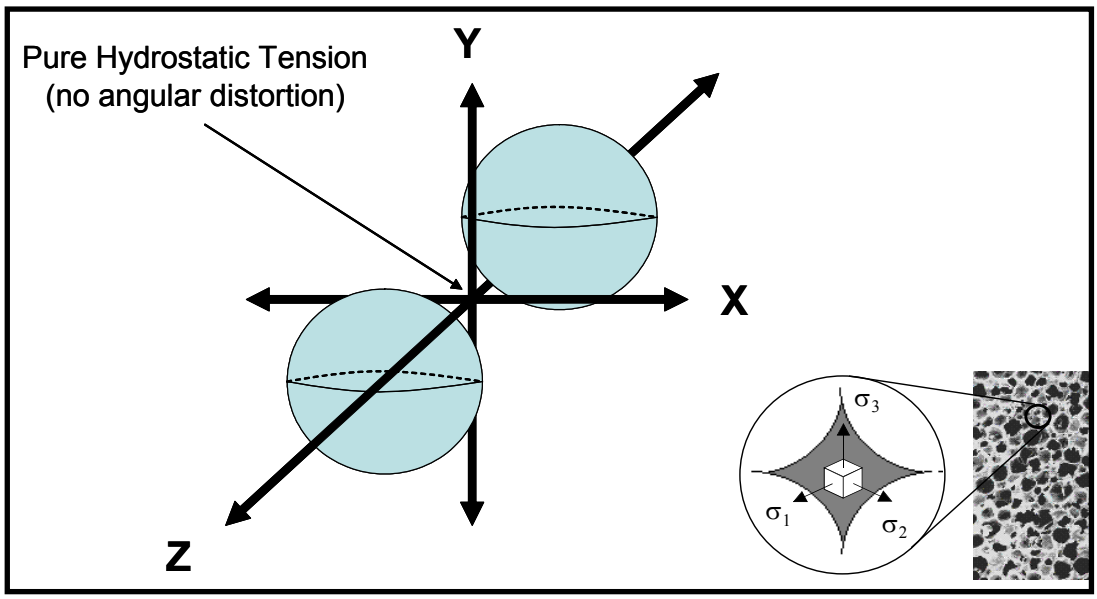

Figure 4.5: Triaxial Tension Requires All Three Axes Unobstructed

In order to obtain some insight into the height (from the bubble surface) of this angular distortion zone, it is first necessary to review some concepts from solid geometry specific to the hexahedron (cube). More specifically, it is useful to review the concepts of the midradius and the circumradius of a unit cube. Both of these concepts are very

useful in building a model of the angular distortion zone which surrounds every bubble in an HPR^{TM} inner matrix. See Figure 4.6 below for an illustration of these concepts [20]. The midradius represents the radius of a sphere (centered inside the unit cube) who's surface just contacts the midpoint of each edge of that unit cube. The circumradius represents the radius of a sphere (centered inside the unit cube) who's surface just contacts each vertex (corner) of that unit cube. Note: The inradius of a unit cube represents the radius of a sphere (centered inside the unit cube) who's surface just contacts the center of each face of that unit cube. In other words, the midradius of a unit cube is the center – edge distance, and the circumradius is the center – vertex distance. Note: Similarly, the inradius of a unit cube is the center – face distance.

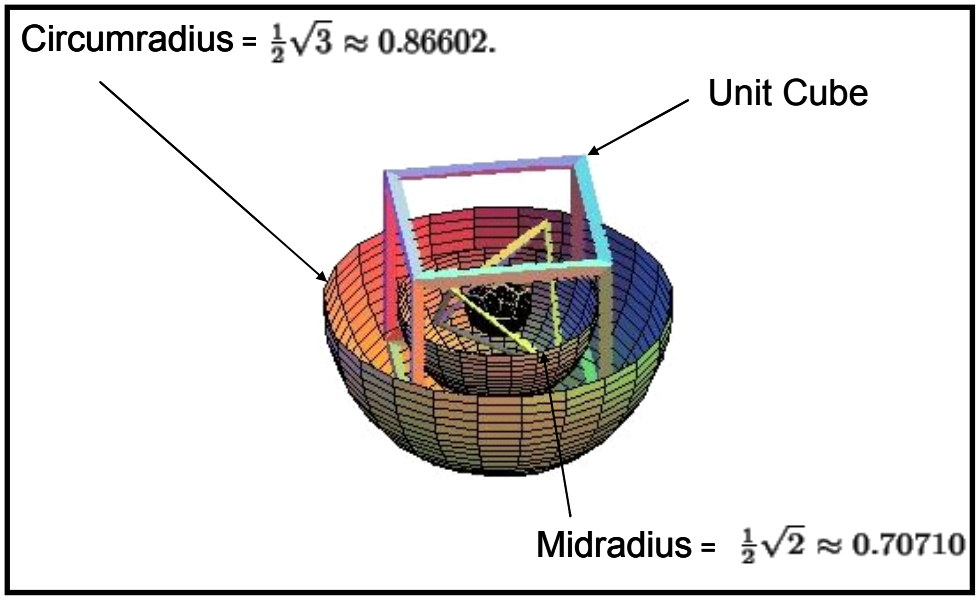

Figure 4.6: Midradius & Circumradius Illustrated

Fresh from that little review we quickly turn our attention to Figure 4.7 below illustrating the requirement for non-obstruction on all three axes, to now recognize that

for a bubble whose radius is represented by the midradius of some unit cube, its associated angular distortion zone has a radius represented by the circumradius of that same unit cube. This convenient geometric relationship allows for the radius of any spherical bubble's angular distortion zone to be to be linearly related to that bubble's own radius.

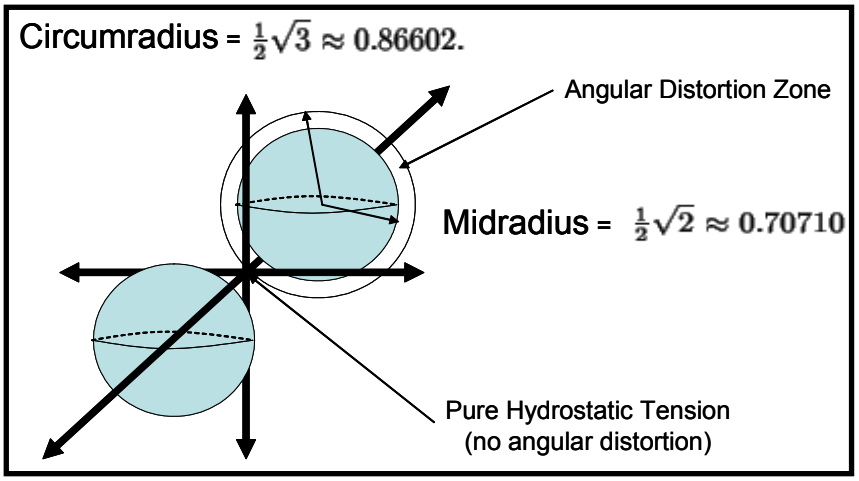

Figure 4.7: Midradius & Circumradius as Related to the Angular distortion zone

The relationship derived here, and shown below in Figure 4.8, for the radius of the angular distortion zone: $r_{ADZ} = 1.2247\ r_{BUBBLE}$ is universally applicable to any and all spherical bubbles in HPR™ inner matrices.

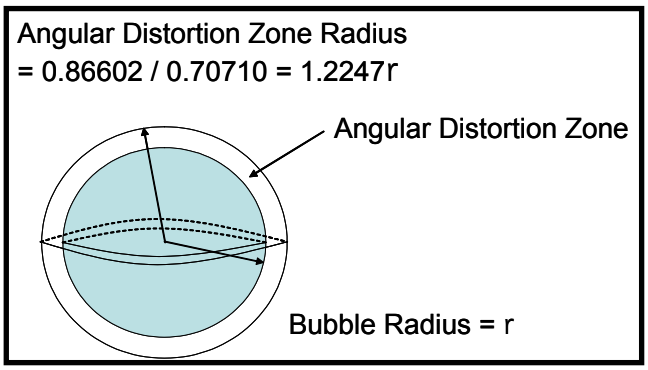

Figure 4.8: Relationship Between Bubble Radius & Angular distortion zone Radius

4.3 Finite Element Method

As shown in Figure 4.9 below, the effect of angular distortion on maximum stress is vividly illustrated by a Finite Element Method (FEM) analysis of a simple one bubble HPR^{TM} inner Matrix using ANSYS3D [21].

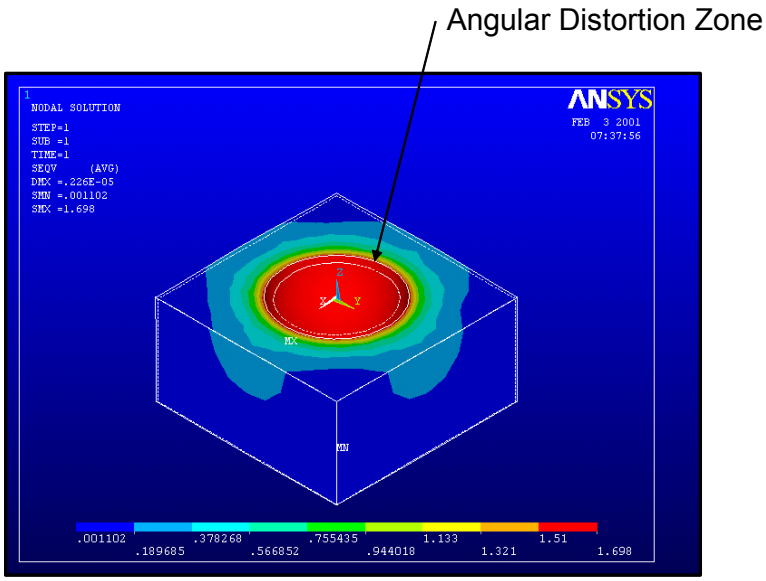

Figure 4.9: Effects of Angular Distortion in a One Bubble HPR^{TM} Inner Matrix [21]

Figure 4.10 below shows the results of a parametric analysis relating the maximum stress to the distance from the bubble expressed as a percentage of that bubble's diameter. Therefore, the angular distortion zone (= 1.2247 r) would extend between the surface of the bubble and ((1.2247 – 1)/2) = 11.23% of its diameter. Just as we expect to see, the maximum stress is relatively constant and unaffected by the bubble outside of the angular distortion zone. These areas are subjected to substantially distortion-free triaxial (hydrostatic) tension. But, inside the angular distortion zone, the maximum stress is dramatically effected by the bubble.

L/D %	L	D	Max Vonmise (Ksi)
1.00%	0.063	6.3	46.645
2.00%	0.063	3.15	21.952
3.00%	0.063	2.1	14.359
4.00%	0.063	1.575	10.412
5.00%	0.063	1.26	7.858
6.00%	0.063	1.05	6.587
8.00%	0.063	0.7875	4.674
10.00%	0.063	0.63	3.644
20.00%	0.063	0.315	2.197
30.00%	0.063	0.21	1.926
40.00%	0.063	0.1575	1.797
50.00%	0.063	0.126	1.723
60.00%	0.063	0.105	1.688
70.00%	0.063	0.09	1.668
80.00%	0.063	0.07875	1.633
90.00%	0.063	0.07	1.626
100.00%	0.063	0.063	1.594

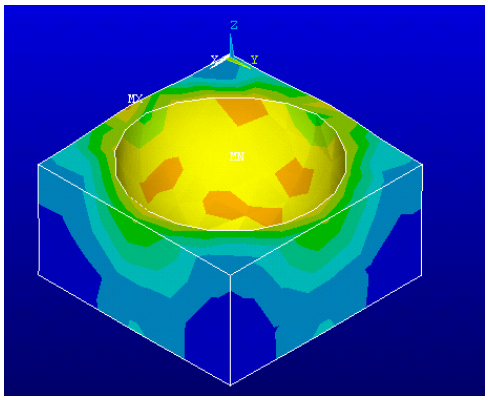

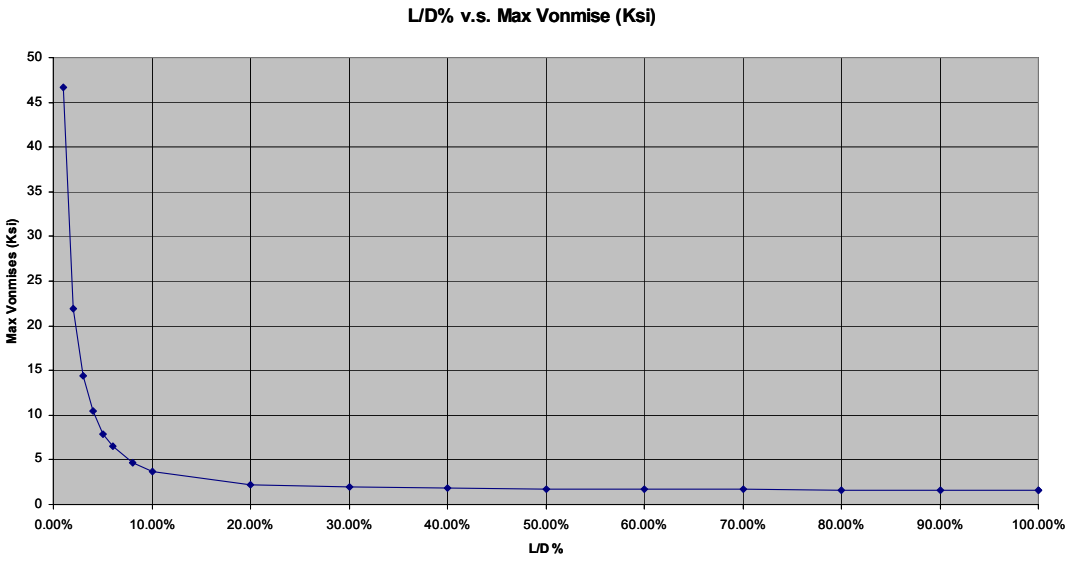

Figure 4.10: Parametric Analysis [21]

The same FEM analyses were performed on an HPR^{TM} inner matrix with multiple bubbles to further verify the expected results. See Figures 4.11 & 4.12 below. The areas which indicated the very highest maximum stresses, are the areas where two or more angular distortion zones intersect with one another. As in the single bubble case above, areas outside the angular distortion zones are relative unaffected by the bubbles. Again, these areas are subjected to substantially distortion-free triaxial (hydrostatic) tension.

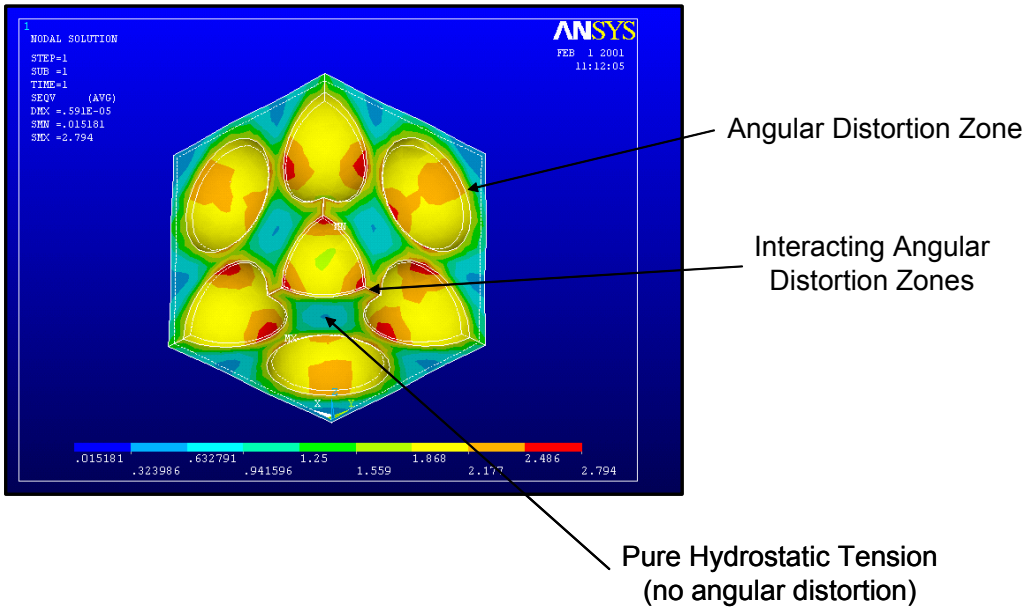

Figure 4.11: Effects of Angular Distortion in a Multi-Bubble HPR™ Inner Matrix [21]

		Max Vonmise (Ksi)		
Void %	L/D	DIA = 0.05	DIA = 0.1	DIA = 0.25
50.00%	1.16%	40.558	40.566	40.514
45.00%	3.88%	11.567	11.584	11.534
40.00%	7.04%	5.987	5.965	5.964
35.00%	10.78%	3.902	3.904	3.89
30.00%	15.30%	3.262	3.244	3.27
25.00%	20.96%	2.794	2.828	2.804
20.00%	28.37%	2.441	2.436	2.412
15.00%	38.77%	2.164	2.317	2.176
10.00%	55.23%	1.999	1.973	1.955
5.00%	89.09%	1.814	1.768	1.772

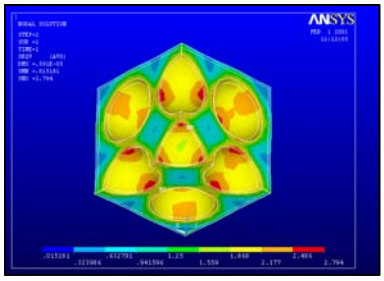

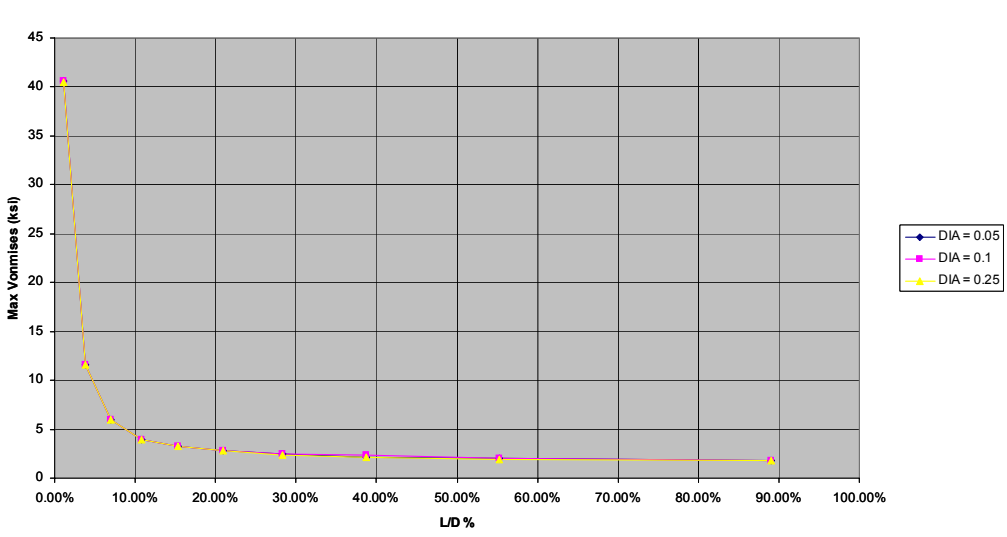

Figure 4.12: Parametric Analysis [21]

Finally, in order to verify the ANSYS3D results, the same conditions were analyzed using LSDYNA3D where similar results were generated. See Figure 4.13 below.

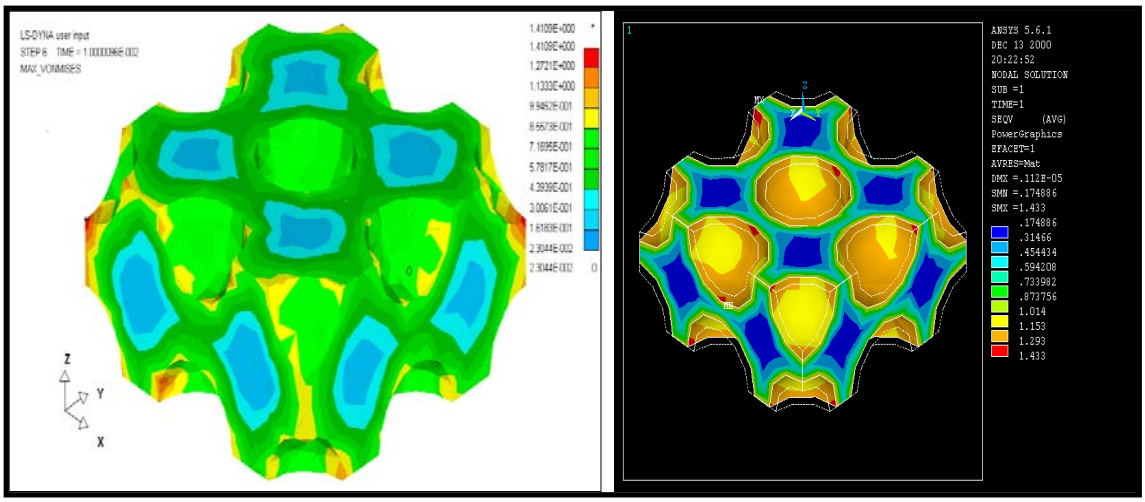

Figure 4.13: LSDYNA and ANSYS Generated Similar Results [21]

4.4 Summary

Investigation reveals that the inner matrix microstructure has a major effect on HPR^{TM} efficiency. The key variable parameters that determine the quality of the inner matrix microstructure from an HPR^{TM} efficiency perspective are as follows; bubble shape distribution/homogeneity, bubble size distribution/homogeneity, bubble position (packing structure) distribution/homogeneity, and bubble spacing distribution/homogeneity. By definition, HPR^{TM} is based on maximizing the occurrence of tri-axial tension in the structural material, which as described herein requires the minimization of zones where angular distortion occurs. Generally, this requires symmetry and homogeneity to be preferred characteristics of an inner matrix microstructure. So, in order to minimize the

zones where angular distortion occurs, spherical bubbles of a single size shall be assumed as ideal for reasons of symmetry and homogeneity, with a smaller (rather than larger) bubble size preferred. Furthermore, a face centered cubic bubble packing structure shall be assumed as ideal. Finally, a bubble spacing that minimizes interference between adjacent angular distortion zones shall also be assumed to be ideal.

CHAPTER 5. METHOD AND RESULTS

Using an existing fabrication technology, several bench scale prototype HPR™ pressure vessels were produced. These vessels were subjected to a variety of tests in an effort to verify the expected performance improvements. Fabrication and testing was accomplished through the kind assistance of Fraunhofer and British Oxygen Company.

British Oxygen Company (BOC) is the world's second largest industrial gas supplier, and the world's first largest customer for pressure vessels. BOC reports annual sales of over $7.3 billion [22]. Testing of the HPR™ pressure vessels was conducted at BOC's Fabrication Technology Centre located in Wolverhampton, UK, by the engineers and technicians of BOC Gases, which is a wholly owned subsidiary of BOC Group with headquarters in Windlesham, Surrey, UK. All costs associated with testing the bench scale prototypes were absorbed by BOC.

Fraunhofer is a non-profit research and development company with locations all over the world. Fraunhofer's total annual research and development budget exceeds $1 billion [23]. The bench scale prototype HPR™ pressure vessels used for this project were fabricated by the engineers and technicians of The Fraunhofer Center for Manufacturing and Advanced Materials, located in Newark, Delaware. The Fraunhofer Center for Manufacturing and Advanced Materials is a part of Fraunhofer USA, which is a wholly owned subsidiary of The Fraunhofer-Gesellschaft, headquartered in Munich,

Germany. A portion of the cost associated with fabricating these bench scale prototypes was covered by BOC. All remaining costs were absorbed by Fraunhofer.

5.1 Fraunhofer Fabrication Method

Based on results from the industry survey, the Fraunhofer style metal foam was selected for use as the HPR^{TM} inner matrices. Besides offering a nearly ideal microstructure, the Fraunhofer fabrication technology offered the additional benefit of creating its own solid outer surface covering. The Fraunhofer method results in a foam product whose cellular microstructure is self-forming. In other words, no precursor or space filler is required. The Fraunhofer method is described in detail in its patent entitled "Methods for Manufacturing Foamable Metal Bodies" [24], originally patented by the Fraunhofer-Institute in Bremen, Germany.

As discussed briefly before, metal powders (elementary metals, alloys, or powder blends) are mixed with a foaming agent and compacted to produce a dense semi-finished product referred to as a foamable precursor. Compaction methods include uniaxial compression, extrusion and powder rolling. When the precursor is heated, the foaming agent decomposes and the released gas forces the melting material to expand (see Figure 5.1 below). The foam parts generally have a dense surface skin with relative densities ranging from 20 - 40 % [25].

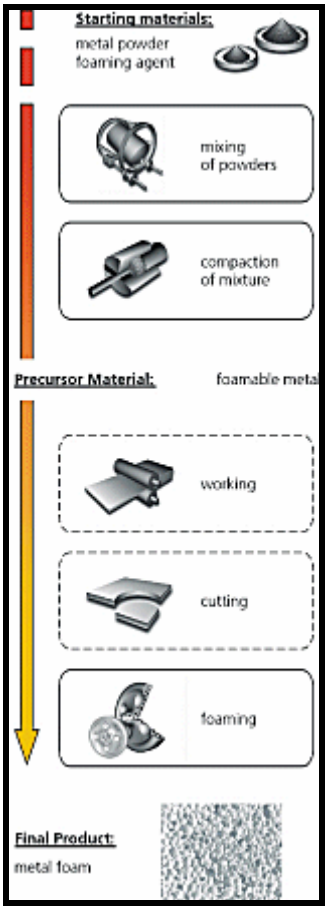

Figure 5.1: Fraunhofer Method [25]

Prior to foaming, the precursor material can be processed into sheets, rods, profiles, etc., by conventional techniques. Near-net shaped parts are prepared by inserting the precursor material into a mold and expanding it by heating. However, by injecting the expanding foam into the molds, quite complicated parts can be manufactured, and improved uniformity of the microstructure is observed. Sandwich panels consisting of a foamed metal core and fully dense face sheets can be obtained by gluing the face sheets to a sheet of foam. Alternatively, a metallurgical bond is achieved by roll-cladding a sheet of foamable precursor material with conventional aluminum or

steel sheets. Figure 5.2 below illustrates the variety of complex 3-dimensional shapes that can be fabricated with the Fraunhofer method.

Figure 5.2: Complex 3-Dimensional Parts [25]

In summary, the Fraunhofer method is moderately economical, results in a product that exhibits a relatively low proportion of microstructural imperfections, and is compatible with production of complex 3-dimensional shapes.

5.2 BOC Testing Method

Bench scale HPR^{TM} pressure vessels were subjected to testing at the BOC labs to determine two critical characteristics, interconnectivity between the individual bubbles of the inner matrices, and burst pressure. Both regimens were conducted at BOC's Fabrication Technology Centre.

5.2.1 Bubble Interconnectivity Test Method

Bubble interconnectivity was measured indirectly by measuring the actual open pore volume of the vessels and then comparing this to the expected open pore volume based on the inner matrix relative densities [26]. The test apparatus designed and built by BOC consisted of the following:

1. A reservoir consisting of a Hoke 500mL-cylinder
2. A pipe system consisting of Swagelok fittings, Hoke Valves, and ¼" stainless steal tubing
3. A 12" pressure gauge -1-4 barg calibrated (readability = 0.05 bar)
4. An Edwards RV3 vacuum pump
5. Oxygen-free nitrogen
6. An HPR™ pressure vessel

Figure 5.3 below shows a schematic of the test apparatus.

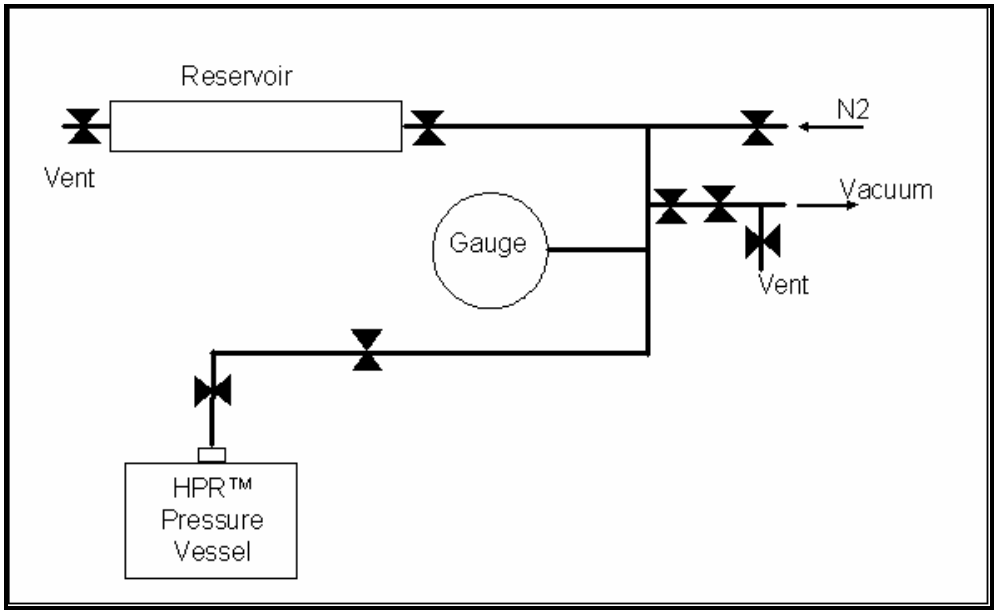

Figure 5.3: BOC Bubble Interconnectivity Test Apparatus Schematic [26]

First the known volumes were determined as follows. The reservoir volume was measured by filling with water and was found to be 513 cc. The pipe-system volume, from the N_2 supply valve to the vacuum pump valve and up to the HPR™ pressure vessel valve, was measured by pressure differential and found to be 27.87 cc. The connector (1cc) plus tube nozzle volume of the HPR™ pressure vessel was calculated as 14cc, from dimensions given by Fraunhofer. Then the following test procedure was used [26]:

Step 1. System evacuation. With the HPR™ pressure vessel installed in the gas-tight container, the system was vacuumed for 30 minutes.

Step 2. HPR™ pressure vessel isolation. The HPR™ pressure vessel valve and the vacuum line valve were then closed.

Step 3. System pressurization. The system was then pressurized to 3 bar, and left to stabilize.

Step 4. HPR™ pressure vessel open porosity volume measured. The HPR™ pressure vessel valve was then opened and the drop in pressure recorded after it stabilized (about 10 minutes).

Constant temperature was assumed so PV = Constant, and the following formula was used: (vol reservoir + vol pipe) x filling pressure = (vol reservoir + vol pipes +vol HPR™ pressure vessel open pores) x final pressure.

The bubble interconnectivity test success criteria set at 90%.

Figure 5.4 below shows a photograph of the test apparatus used by BOC.

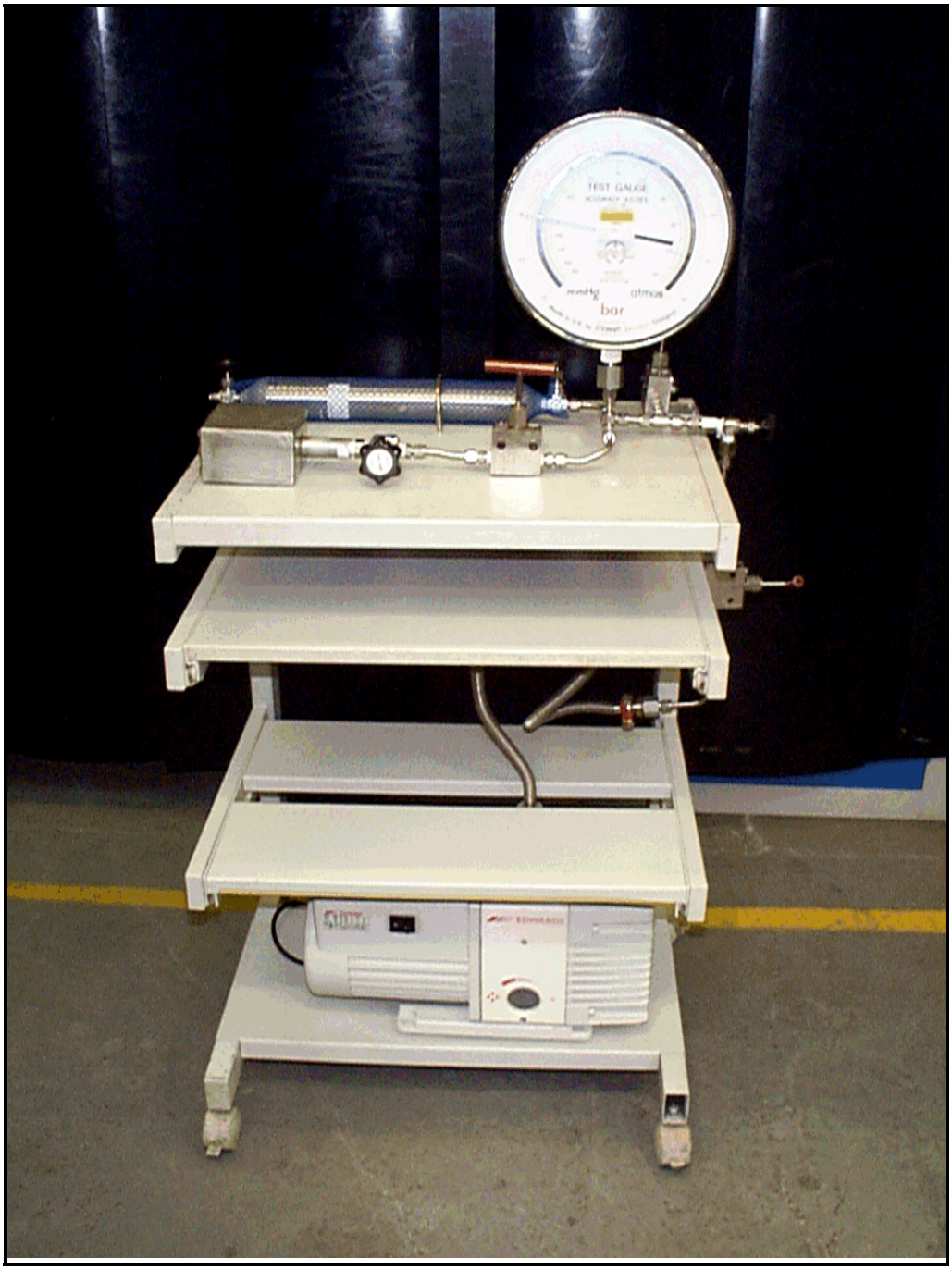

Figure 5.4: Test Apparatus used by BOC [26]

5.2.2 Burst Pressure Test Method

Burst pressures were measured by applying pressurized nitrogen to the HPR™ pressure vessels and slowly increasing the pressure until each vessel failed [27]. The test apparatus designed and built by BOC consisted of the following:

1. A nitrogen cylinder (200bar)
2. A high flow high pressure regulator (L800 160 bar)
3. A high pressure gauge (0-160 bar, Budenberg)
4. A pipe system consisting of Swagelock fittings, Hoke Valves, and ¼" & 2mm stainless steal tubing
5. blast wall cubicle, open air
6. plastic water tank
7. video equipment with remote monitor
8. An HPR™ pressure vessel

Figure 5.5 below shows a schematic of the test apparatus.

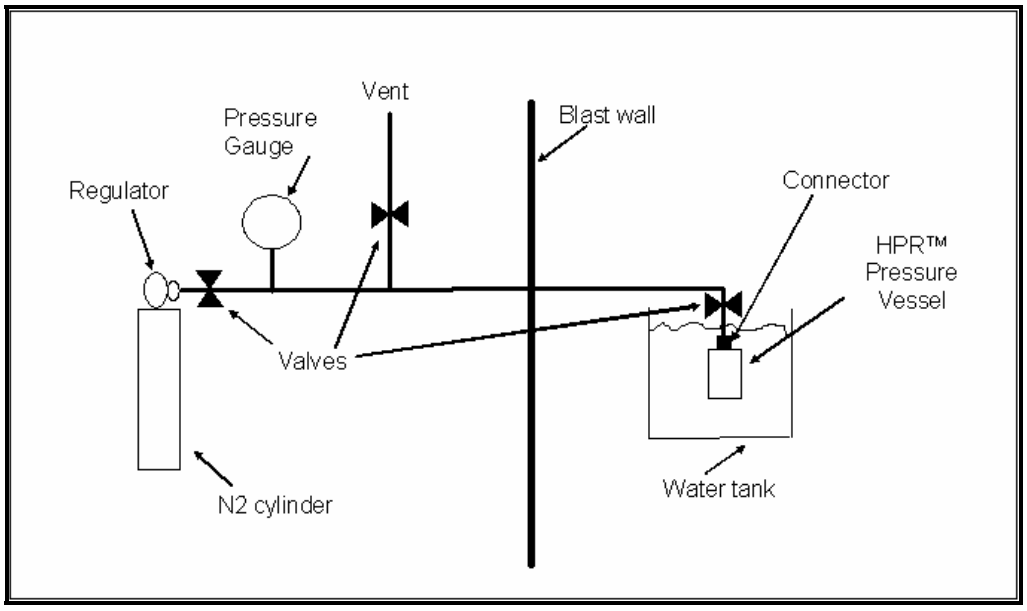

Figure 5.5: BOC Burst Test Apparatus Schematic [27]

The following safety precautions were observed during the conduct of all burst tests due to the use of high pressures. All operators were required to work from outside the blast wall. No personnel were allowed inside the blast wall when the system was pressurized. The burst tests were observed through a port in the blast wall, with a remote monitor so that the operator could see what is happening from outside the blast wall. The outlet of the vent was fitted and directed well away from operators. The HPR^{TM} pressure vessel was be submerged in water to record when the gas starts leaking. Operators were required to wear safety glasses, safety boots and laboratory coats. The following test procedure was used [27]:

Step 1. The equipment was first tested for leaks by pressurizing the system with nitrogen without the HPR^{TM} pressure vessel.

Step 2. HPR^{TM} pressure vessel pressure determination. The HPR^{TM} pressure vessel was fitted to the system and placed inside the water tank. The system was then slowly pressurized (in steps of 1bar) and the pressure recorded when bubbles start to form, as when seen in the video monitor. The pressure was then released down to atmospheric.

Step 3. HPR^{TM} pressure vessel burst pressure determination. The water tank was taken away and the system was pressurized (steps of 5 bar). The

pressure was recorded when the first burst occurred. The pressure was then released down to atmospheric.

Step 4. HPR™ pressure vessel complete rupture pressure determination. The system was pressurized in steps of 5 bar up to the bursting pressure, then it was pressurized further until complete rupture occurred.

The burst test success criteria was set at a minimum burst pressure of 1000psi, and a desired burst pressure greater than or equal to 1,500psi.

5.3 Test Results

Three sets of HPR™ pressure vessels were fabricated by Fraunhofer to support testing by BOC. All three sets of pressure vessels were of the same general dimensions. The bench scale HPR™ pressure vessels prototypes were watch-box sized vessels measuring 4" x 4" x 1" with a fill tube installed in the center of one 4" x 4" side. The first set of HPR™ pressure vessels had no additional outer covering. The second set had an epoxy based resin coating added for improved hermetic sealing. And, the third set had a sheet aluminum outer surface added on for even better hermetic sealing. The results from testing each set of HPR™ pressure vessel are discussed in detail. Figure 5.6 below shows one of the prototypes from the first set.

Figure 5.6: Bench Scale Prototype HPR^{TM} Pressure vessel [28]

5.3.1 Test Results - Set One

As shown in Figure 5.6 above, the first set of 12 prototypes were fabricated without any special coating on the outside surface of the vessels [28]. It was the initial expectation that the self forming solid outer surface would be hermetically sealed by itself. However, when BOC attempted to perform the bubble interconnectivity test, it was found that the outer surface was not hermetically sealed. In fact the outer surface was permeated by many microscopic passages that allowed the gas molecules to escape at even slight pressures. Therefore, bubble interconnectivity testing could not be accomplished on set one. It was decided however to conduct one burst test, by quickly filling the HPR^{TM} pressure vessel in an effort to "overwhelm" the leak rate. This method worked, and the result was quite successful. The HPR^{TM} pressure vessel burst at a pressure of 1,800psi; well above the minimum required pressure of 1,000psi, and the

desired pressure of 1,500. So, while the outer surface permeability issue was discouraging, the burst pressure result seemed to be an immediate validation of the basic HPR^{TM} principle.

5.3.2 Test Results - Set Two

The second set of 12 prototypes were fabricated identically to the first set, except that an epoxy coating was applied to the outer surface of each vessel in an effort to improve the hermetic seal of the outer surface. As each vessel was dipped in the liquid epoxy, a vacuum was drawn to help ensure a best possible bond.

5.3.2.1 Bubble Interconnectivity Test results

Six of the 12 prototypes were selected for bubble interconnectivity testing base on a visual observation of the quality of the epoxy coatings. Bubble interconnectivity testing was successfully accomplished on all six of the HPR^{TM} pressure vessels, yielding results that are shown in Table 5.1 below [29].

	BOC Measurements				
HPR Pressure Vessel	Total pore volume as %of vessel volume	Vessel total volume (cm3)	Open pore volume measured (cm3)	Open pore volume as % of vessel total volume	Open pore volume as % of total pore volume
1	77.4	626.2	475.2	75.9	98
2	79.4	626.2	479.1	76.5	96.4
4	78.5	626.2	407.1	65	82.8
5	76.2	626.2	442.5	70.7	92.7
9	76.1	626.2	431.9	69	90.6
10	77.5	626.2	439.4	70.2	90.6

Table 5.1: Set 2 Bubble Interconnectivity Test Results [29]

Only one vessel failed to meet the minimum requirement of 90%. It is hypothesized that the very same mechanism that causes the untreated outer surface to be permeable, also facilitates the high degree of bubble interconnectivity. Some characteristic of the Fraunhofer foaming process results in the solid portion of the aluminum material to be infiltrated with a multitude of microscopic passages. In terms of inner matrix bubble interconnectivity; this characteristic is a very fortunate circumstance for the fabrication of HPR^{TM} pressure vessels.

5.3.2.2 Burst Pressure Test Results

Burst pressure test results were not so encouraging however. Six HPR^{TM} pressure vessels were selected at random for the destructive burst pressure tests [30]. For all six vessels, the epoxy coatings did not bond as well as expected, resulting hermetic seal failures as the coatings separated from the main bodies of the HPR^{TM} pressure vessels. Tables 5.2 and 5.3 below provide a detailed explanation of the failure modes for two of the vessels. As can be seen, HPR^{TM} pressure vessel 1 failed at 480 psi and HPR^{TM} pressure vessel 5 failed at 595 psi. These results were completely typical. All six of the pressure vessels failed in a similar fashion – none having attained the minimum required pressure of 1,000 psi.

Unfortunately, the video recording system failed too. So, there are no video records to study. There are however, still photographs (Figures 5.7 and 5.8 below) of the ruptured HPR^{TM} pressure vessels which can be used to study the results. Clearly visible

is a large void which was bisected by the rupture line through the inner matrix of this vessel. All of the vessels tested had similar voids in their inner matrices. Microstructural defects such as these were the cause of the burst pressure failures in Test Set Two.

Applied Pressure (psi g)	**Visual Inspection**	**Comments**
HPR™ pressure vessel 1		
increase pressure gradually to		
15	leak at one corner	sample in water
pressure released to ambient		water bath out
increase pressure in steps of 75		
75	noise from resin break	sample in air
150	noise from resin break	sample in air
225	noise from resin break	sample in air
300	noise from resin break	sample in air
375	noise from resin break	sample in air
450	noise from resin break	sample in air
~480	noise burst of first hole	sample in air
pressure released to ambient		
increase pressure in steps of 75		
150	no effect	sample in air
225	no effect	sample in air
300	no effect	sample in air
375	no effect	sample in air
450	no effect	sample in air
525	hissing noise	sample in air
~585	loud bang, complete failure of sample	
pressure released to ambient		

Table 5.2: Burst Test Results for HPR™ pressure vessel 1 [30]

Applied Pressure (psi g)	Visual Inspection	Comments
HPR™ pressure vessel 5		
increase pressure gradually to		
30	no effect	sample in water
45	leak at base and top	sample in water
pressure released to ambient		water bath out
increase pressure in steps		
75	no effect	sample in air
150	noise from resin break	sample in air
225	noise from resin break	sample in air
300	noise from resin break	sample in air
375	noise from resin break	sample in air
450	noise from resin break	sample in air
pressure released to ambient	resin peeled off	
increase pressure in steps		
150	no effect	sample in air
300	no effect	sample in air
450	no effect	sample in air
~495	noise, burst of first hole	sample in air
pressure released to ambient		
increase pressure in steps		
150	no effect	sample in air
300	no effect	sample in air
450	no effect	sample in air
525	hissing noise	sample in air
600	hissing noise	sample in air
675	hissing noise	sample in air
~720	loud bang, complete failure of sample	
pressure released to ambient		

Table 5.3: Burst Test Results for HPR™ pressure vessel 5 [30]

Figure 5.7: Large microstructural voids bisected along the rupture line [30]

Figure 5.8: Close-up of microstructural voids [30]

5.3.3 Test Results - Set Three

In order to overcome the two primary failure modes encountered in Test Set Two, outer surface hermetic seal failure, and burst pressure test failure; the following step were taken in Test Set Three [31]:

1. An outer covering of sheet aluminum was metallurgically bonded to the outer surface of the HPR^{TM} pressure vessels.
2. All prototypes were prescreened by X-Ray to eliminate those with visible microstructural voids.

Figures 5.9 and 5.10 below illustrate the configuration of the Test Set Three prototype vessels with an outer covering of sheet aluminum. In order to overcome the passivating aluminum-oxide layer on the sheet metal and the semi-liquid foam, which usually prohibits a diffusion process from obtaining a strong metallurgic bond; an intermediate zinc based metal layer was applied on the aluminum sheets right before the foaming procedure. To further improve the diffusion process a high purity (1100 series) aluminum sheet material was selected for attachment to the AlSi12 aluminum foam body. The procedure used was [31]:

Step 1: Machine 12 Sets of 1100 series aluminum sheets

Step 2: Machine 12 6063-T1 series aluminum tubes

Step 3: Machine 12 pieces of AlSi12 precursor material

Step 4: Coat of all the aluminum parts with a zinc based metal alloy

Step 5: Prepare the box shaped bottom piece for easier handling and better sealing

Step 6: Load the mold with the box-bottom, top plate, tube and foamable precursor

Step 7: Foam the prototype in the furnace

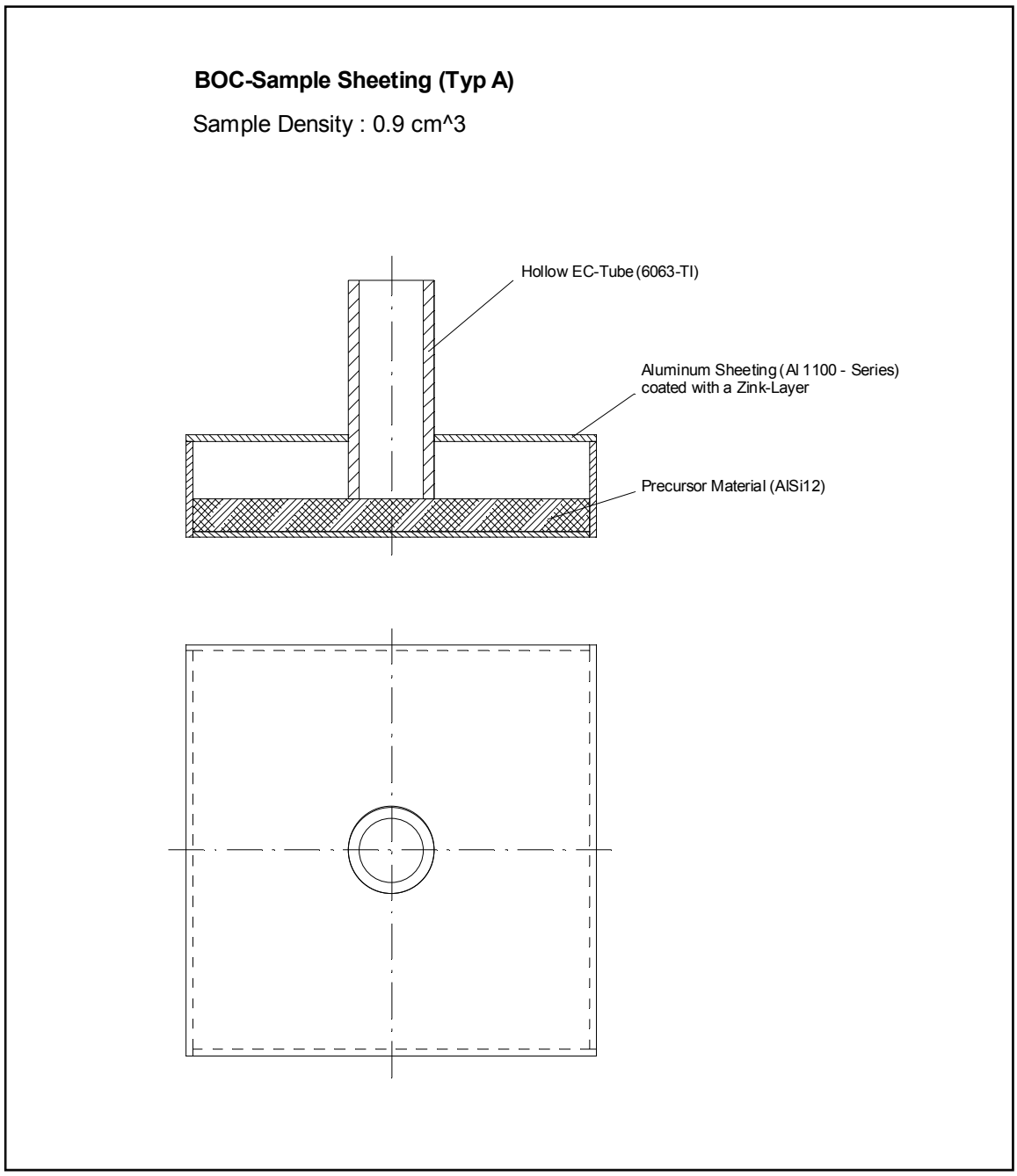

Figure 5.9: HPR^{TM} Pressure Vessel Drawing [32]

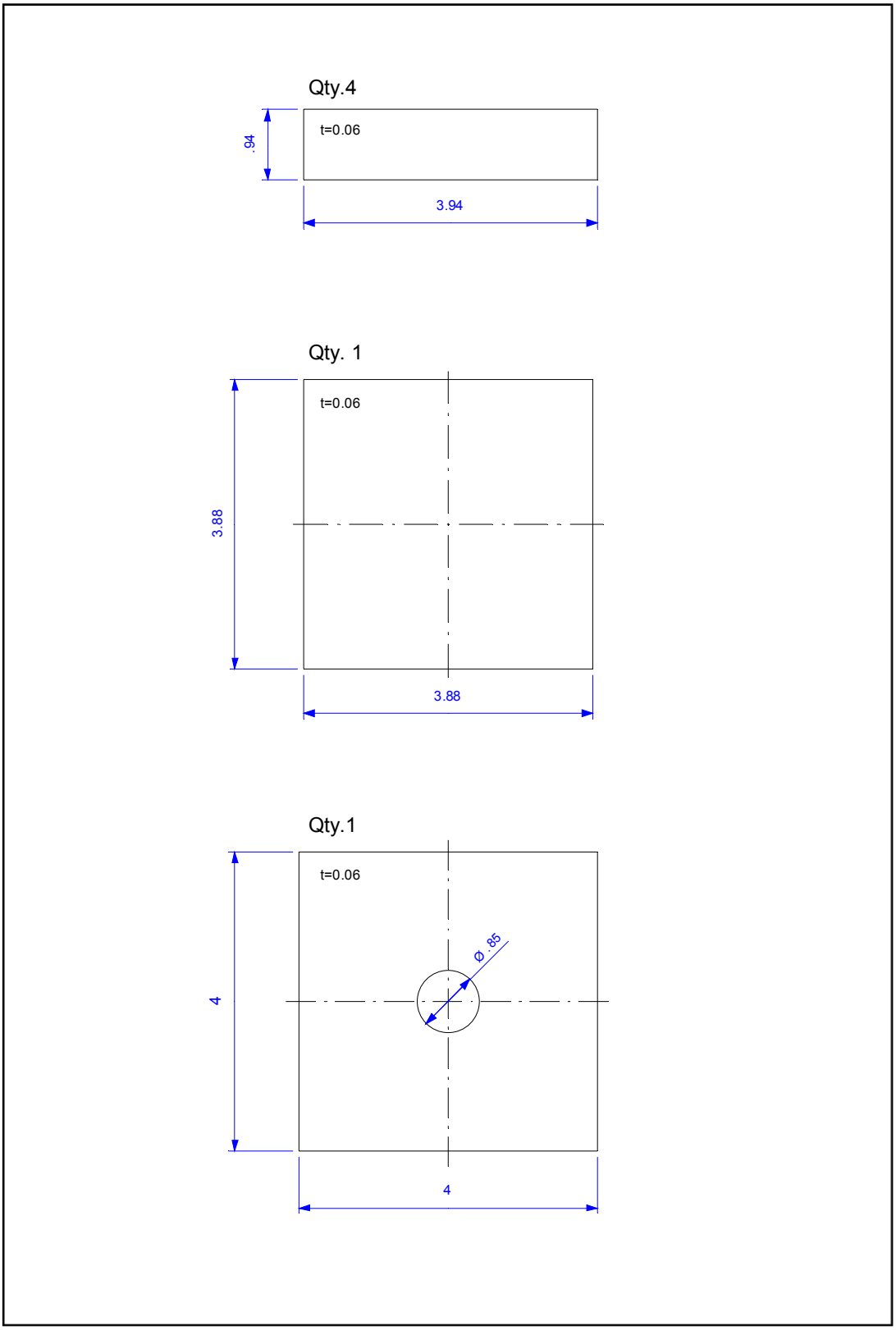

Figure 5.10: HPR^{TM} Pressure Vessel Dimensions [32]

Figures 5.11 and 5.12 below show an example of steps 1 through 5 as listed above.

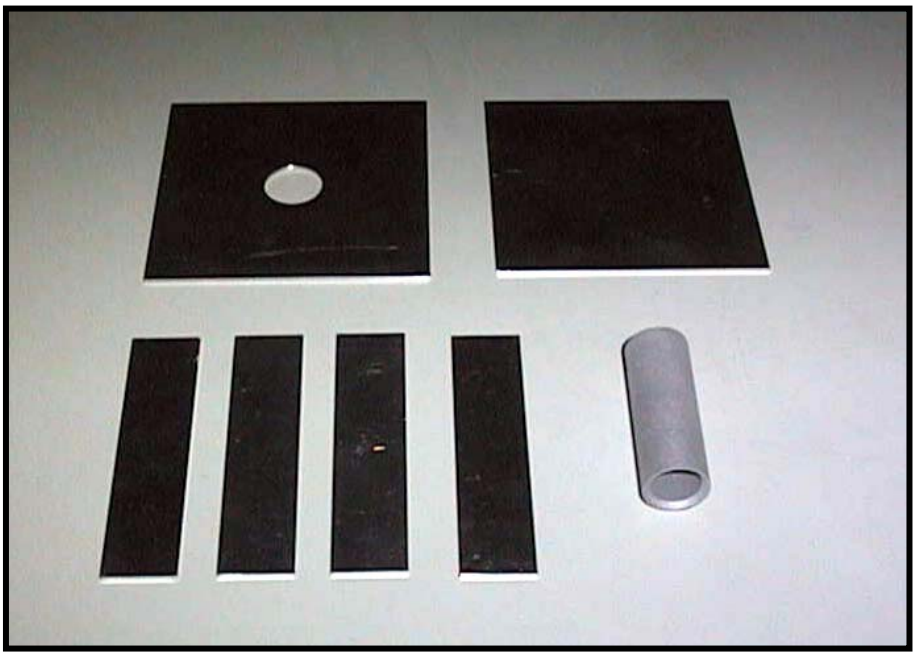

Figure 5.11: HPR™ Pressure Vessel Parts [32]

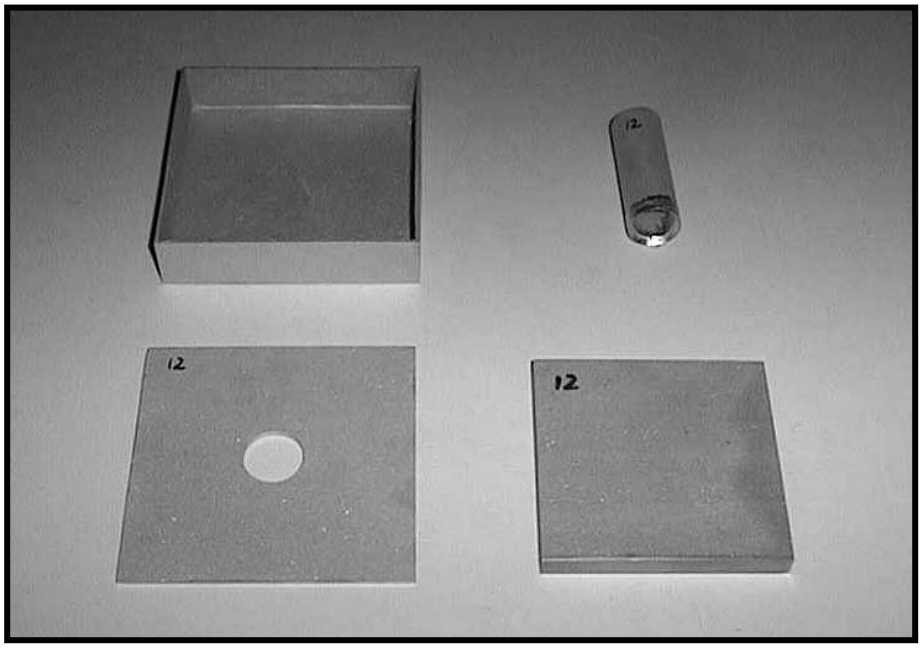

Figure 5.12: HPR™ Pressure Vessel Partially Assembled [32]

Six of the 12 prototypes [32] were selected at random and tested for bubble interconnectivity with all six surpassing 90%. The results are shown below in Table 5.4.

HPR Pressure Vessel No.	Open Pore Volume as a % of Total Pore Volume
BOC 01	96.7%
BOC 02	98.7%
BOC 03	96.9%
BOC 09	98.1%
BOC 11	96.6%
BOC 12	91.0%

Table 5.4: Bubble Interconnectivity Test Results [32]

However, all 12 units failed the burst pressure test with the sheet aluminum cover pieces separating from the main bodies of the vessels at pressures less than 60 psi. That the metallurgical bond between the aluminum sheet material and the HPR^{TM} pressure vessel main bodies failed so totally was a surprise. Figures 5.13 through 5.16 below show several of the failed pressure vessels, bisected to reveal their interior details [32].

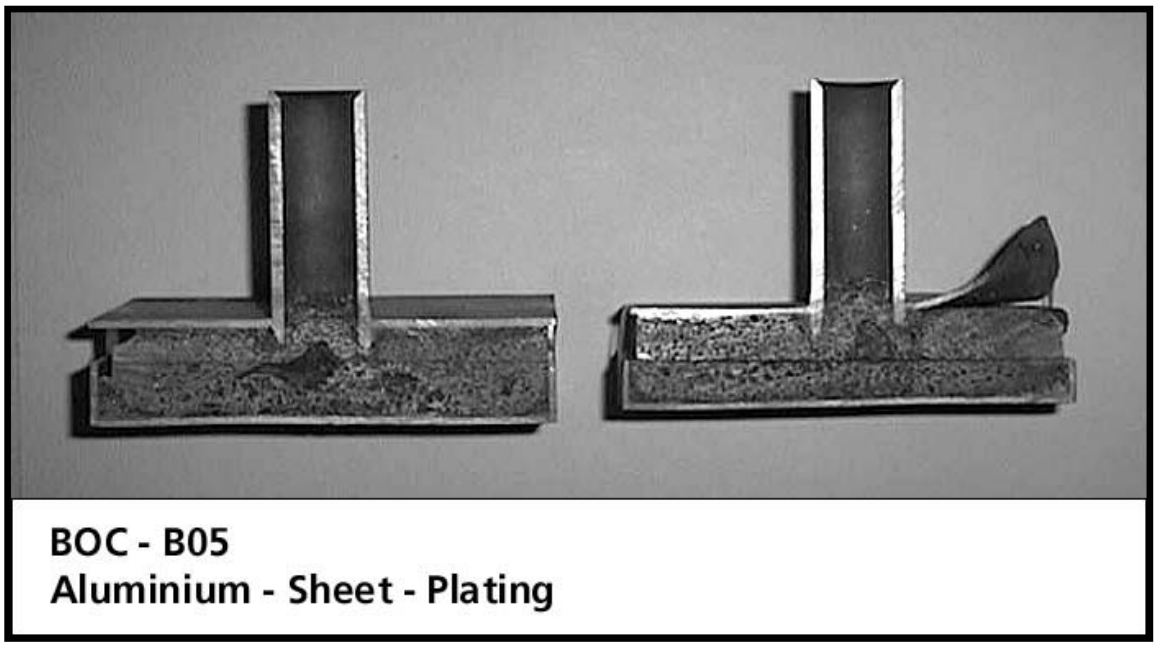

Figure 5.13: HPR^{TM} Pressure Vessel Showing Sheet Aluminum Separation [32]

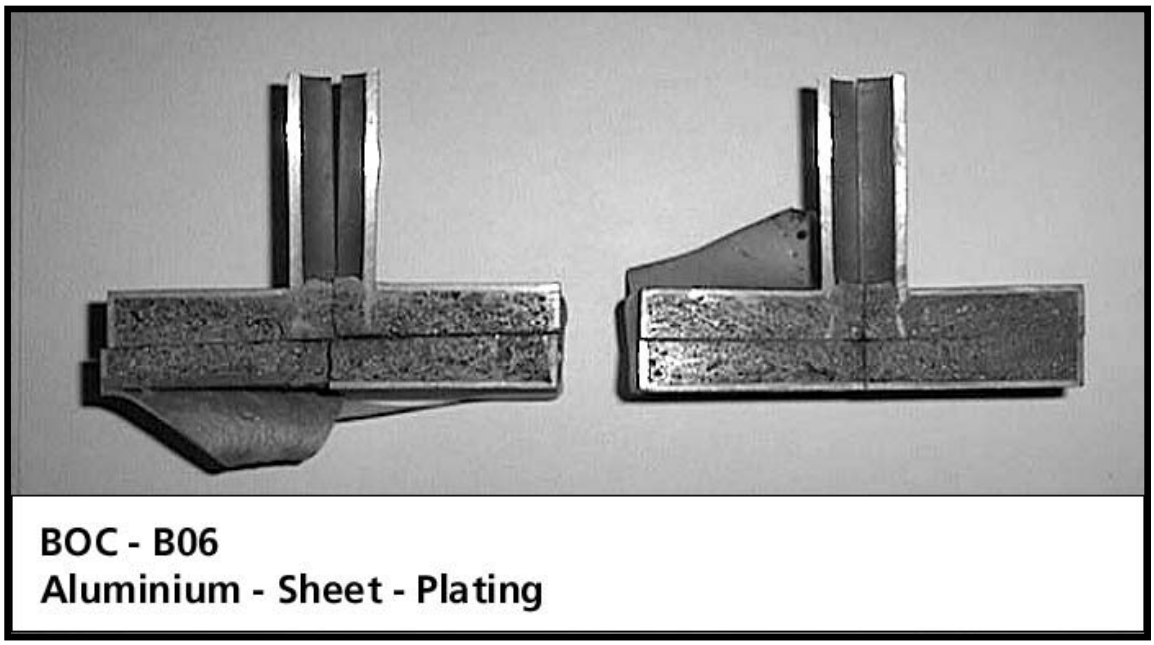

Figure 5.14: HPR^{TM} Pressure Vessel Showing Sheet Aluminum Separation [32]

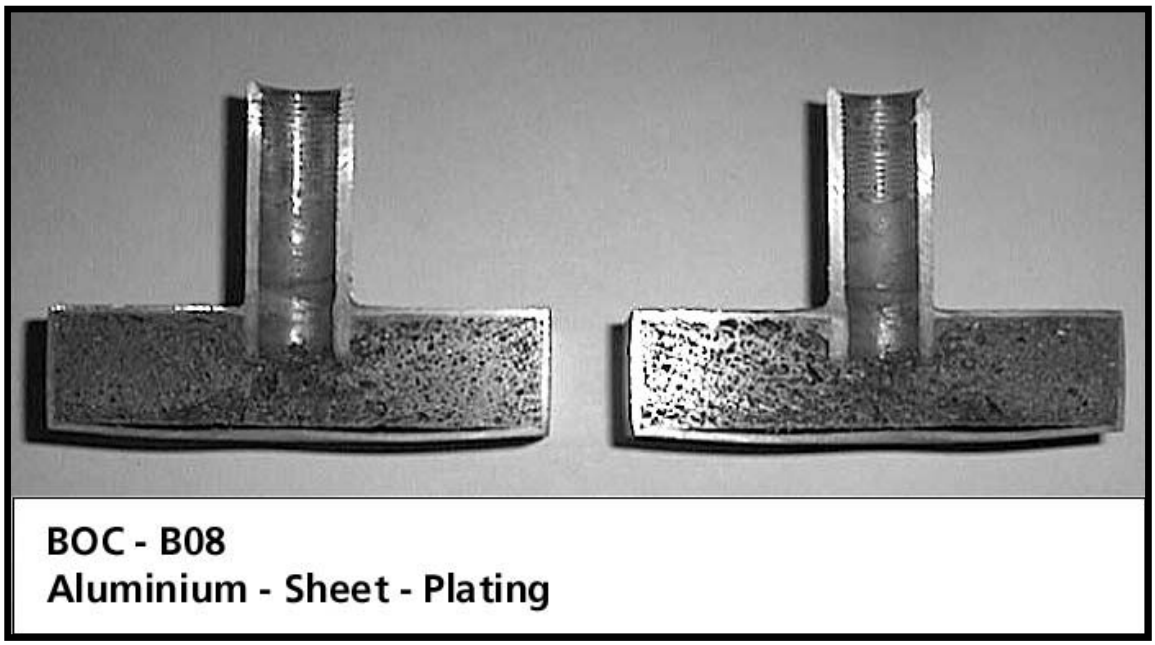

Figure 5.15: HPR™ Pressure Vessel Showing Sheet Aluminum Separation [32]

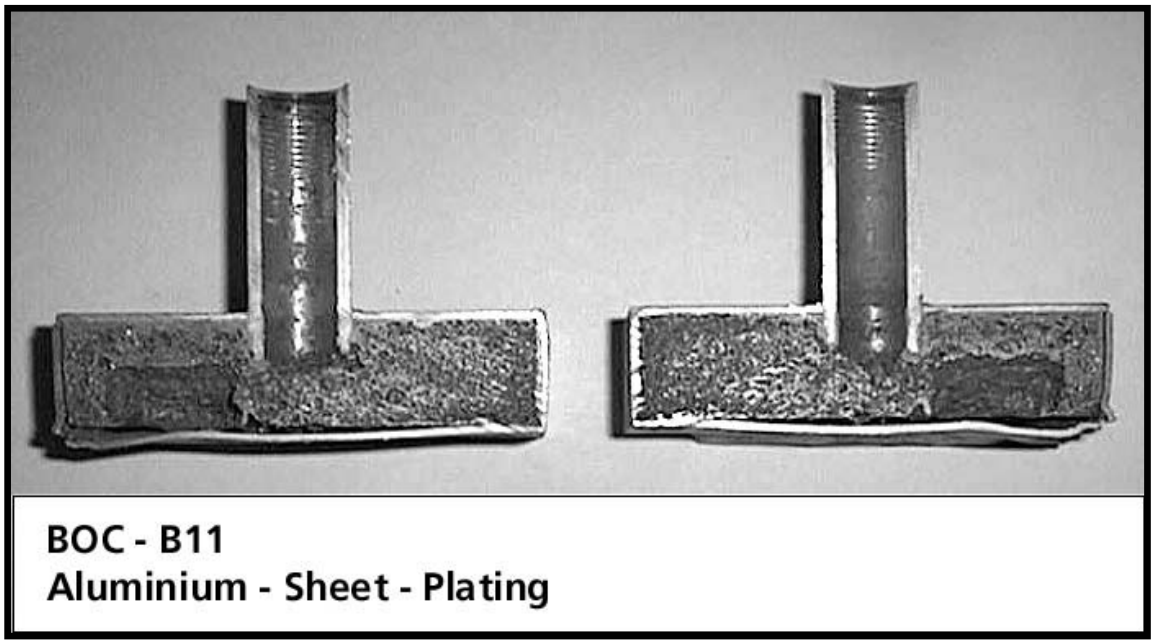

Figure 5.16: HPR™ Pressure Vessel Showing Sheet Aluminum Separation [32]

Two possible reasons for these failures are summarized below [31].

1. Premature zinc diffusion

The average thickness of the manually applied zinc layer was about 10 μm, which was possibly not thick enough to leave enough zinc after application of the foaming temperature of 725 °C. After the zinc diffused into the aluminum sheet it possibly left too little on the surface to inter-react with the foam aluminum main body. Application of a thicker layer of zinc might solve this problem.

2. Permeability of the aluminum oxide layer (Al_2O_3 - barrier)

During application of the zinc based solder material on the aluminum sheet surface, a vibration pen was used to obtain uniform wetting. The existing oxide layer might not have been penetrated thoroughly enough by the mechanical force of the vibrating blade; with the result that the inter-metallic reaction between the zinc and the aluminum was inhibited due to the blocking behavior of Al_2O_3. Chemical preparation of the aluminum by additional non-corrosive fluxes might overcome this problem.

5.4 Summary

Based on the results from all three sets of testing, it can be stated that the Fraunhofer fabrication method resulted in HPR^{TM} pressure vessels that were very difficult to hermetically seal and exhibited generally poor quality microstructures. Both issues dramatically impaired the technical performance of the vessels. As a result, neither success criteria was achieved.

CHAPTER 6. CONCLUSIONS & RECOMMENDATIONS

Based on the results in all three sets of testing it was concluded that the Fraunhofer fabrication method was not suitable for producing HPR^{TM} pressure vessels. Another fabrication method would be required that insures better quality control over the inner matrix microstructure. After conducting another industry survey which included those fabrication methods that have not yet been commercialized, a different fabrication method was selected for possible evaluation [33]. The method selected is called the "Casting Around Space Holders Method".

6.1 The Casting Around Space Holders Method

The casting around space holders method results in a foam product whose cellular microstructure is not self-forming, but is pre-designed [34]. Casting liquid metal around inorganic or even organic granules can produce lightweight porous metals or hollow spheres of low density, or by introducing such materials into a metallic melt. The granules either remain in the metallic product after casting (yielding what is called a ''syntactic foam'') or are removed by leaching in suitable solvents or acids or by thermal treatment (see Fig. 6.1 below). This can be done successfully if the content of space holding fillers is so high that all the granules are interconnected. Vermiculite or fired clay pellets, soluble salts, loose bulks of expanded clay granules, sand pellets, foamed glass spheres or aluminum oxide hollow spheres can serve as inorganic filler material. Polymer spheres can be used as organic space holders if the solidification of the melt is sufficiently fast. The latter requires high-pressure infiltration in a die-casting machine.

The casting around space holders method is very economical, and there is absolute control over the cellular microstructure, resulting in a product that exhibits a very low proportion of microstructural imperfections. It is also compatible with production of complex shapes (see Fig. 6.2 below).

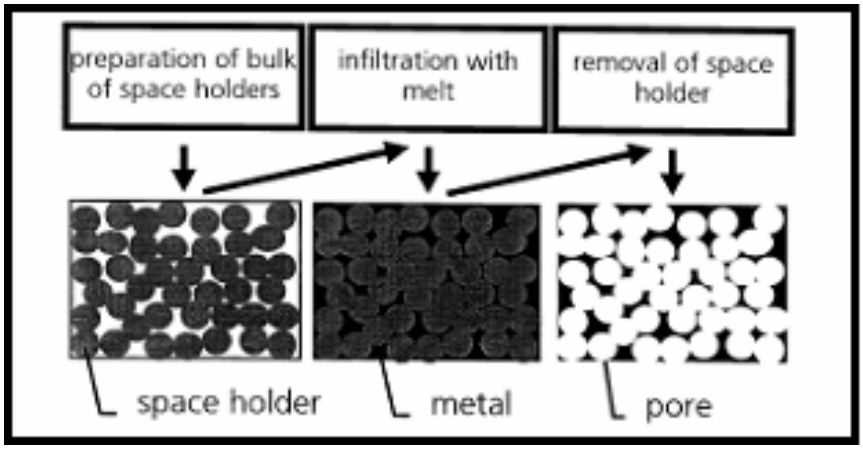

Figure 6.1: Fabrication Process for Casting Around Space Holders

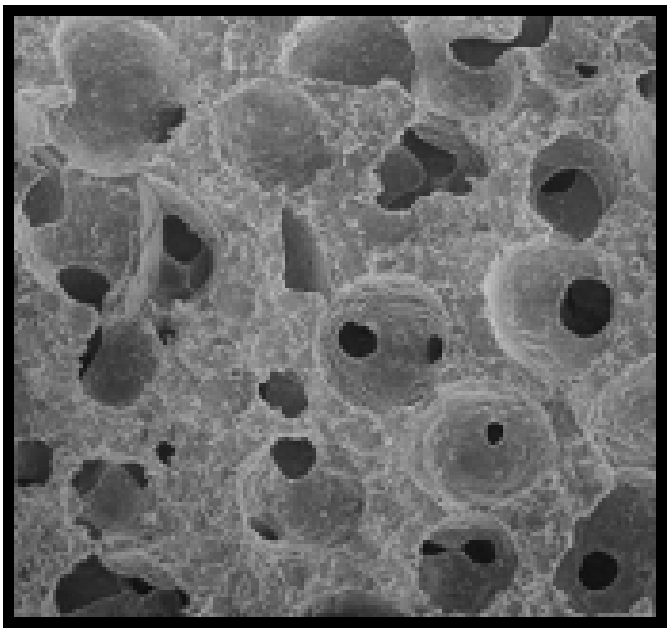

Figure 6.2: Casting Around Space Holders Foam Microstructure

6.2 Supplemental Future Work - Transcryogenic Gas Storage

Large scale industrial storage and transport of gas is often done under cryogenic or liquefied conditions owing to the substantial advantages gained by the resulting reduction in the size and mass of the container for a given mass of gas. This increase in storage efficiency (where storage efficiency is defined as the mass of the stored gas divided by the mass of the storage container) has far reaching beneficial effects, both operational and economic. The basic principle of this advantage appears to apply even to relatively small scale storage and transportation. Most applications, however, involve using these gases while in a gaseous phase at or near ambient conditions, rather than in a cryogenically chilled liquid phase.

'Transcryogenic Gas Storage' another original invention of this author, is defined here to mean; storage of a gas in a special container which involves introducing the gas into the container while in a gaseous phase, then transforming the gas into a liquid or gas/liquid mixture phase by cryogenically chilling the gas inside the container, then transforming the gas back to a gaseous phase upon removal from the container by returning it to ambient conditions. The Transcryogenic Gas Storage process allows for much more efficient storage of the gases than by conventional high pressure storage. Further, the Transcryogenic Gas Storage process occurring inside the special container is autonomous from the user who simply puts a gas into the container and later removes the gas when needed. The user obtains the all the advantages of increased storage efficiency without any loss of operational convenience.

Use of HPR™ pressure vessels affords an opportunity to explore the possible advantages Transcryogenic Gas Storage. HPR™ pressure vessels when designed with structurally supporting inner matrices (see Figure 6.3) which are also thermally conductive uniquely provide an ability to safely store gases at very high pressures under isothermal conditions, as opposed to the adiabatic conditions encountered with conventional pressure vessels. This isothermal condition allows for gases to be introduced into the HPR™ pressure vessel in a gaseous phase under low to moderate pressures and then quickly and efficiently chilled to a liquefied phase for higher density storage. An HPR™ pressure vessel configured for Transcryogenic Gas Storage might also be modified to include a highly thermally conductive artery system within the structural inner matrix to help ensure homogeneous heat removal (see Figure 6.4). The gas is expected to return to the gaseous phase upon removal from the HPR™ pressure vessel due to its return to ambient conditions. By selecting highly efficient insulation for the HPR™ pressure vessel outer surface and an appropriately sized energy efficient cryocooler, Transcryogenic Gas Storage can be a very efficient process. Transcryogenic Gas Storage is probably most suitable for applications where gas is filled into the tank and later removed from the tank rather slowly, as opposed to applications requiring a quick fill or quick release. Depending upon a variety of circumstances, the energy required for Transcryogenic Gas Storage in an HPR™ pressure vessel may be less than the energy required for simple high compression storage at ambient temperatures. Regardless, the storage efficiency of HPR™ pressure vessel can be greatly enhanced by the use of a Transcryogenic Gas Storage process.

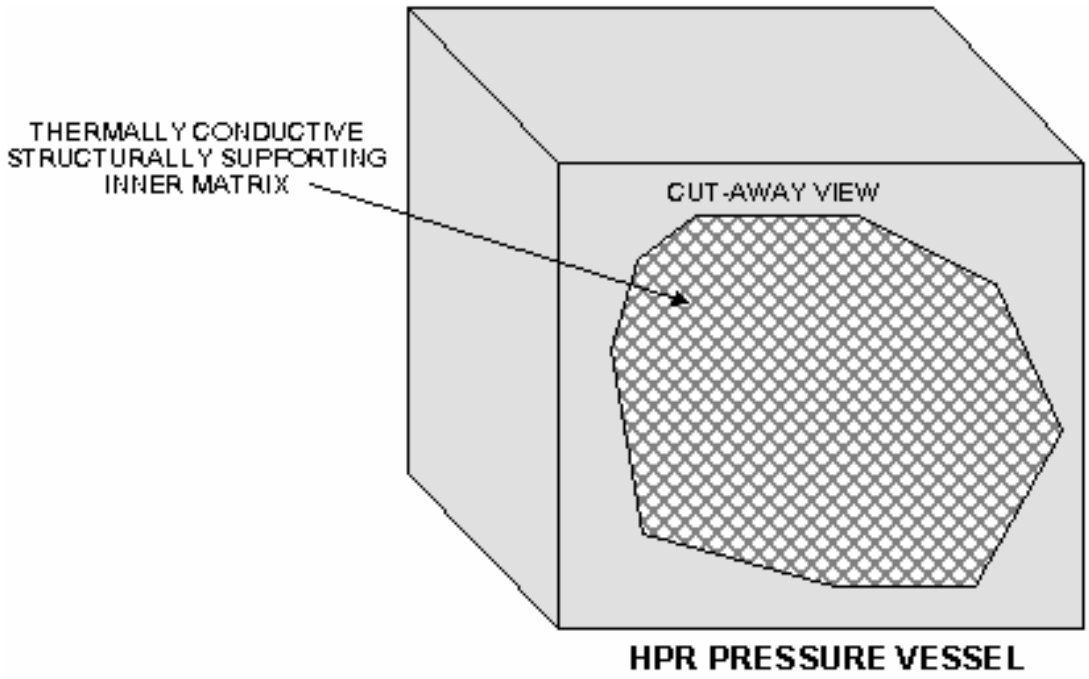

Figure 6.3: An HPR Pressure Vessel with a Thermally Conductive Structurally Supporting Inner Matrix

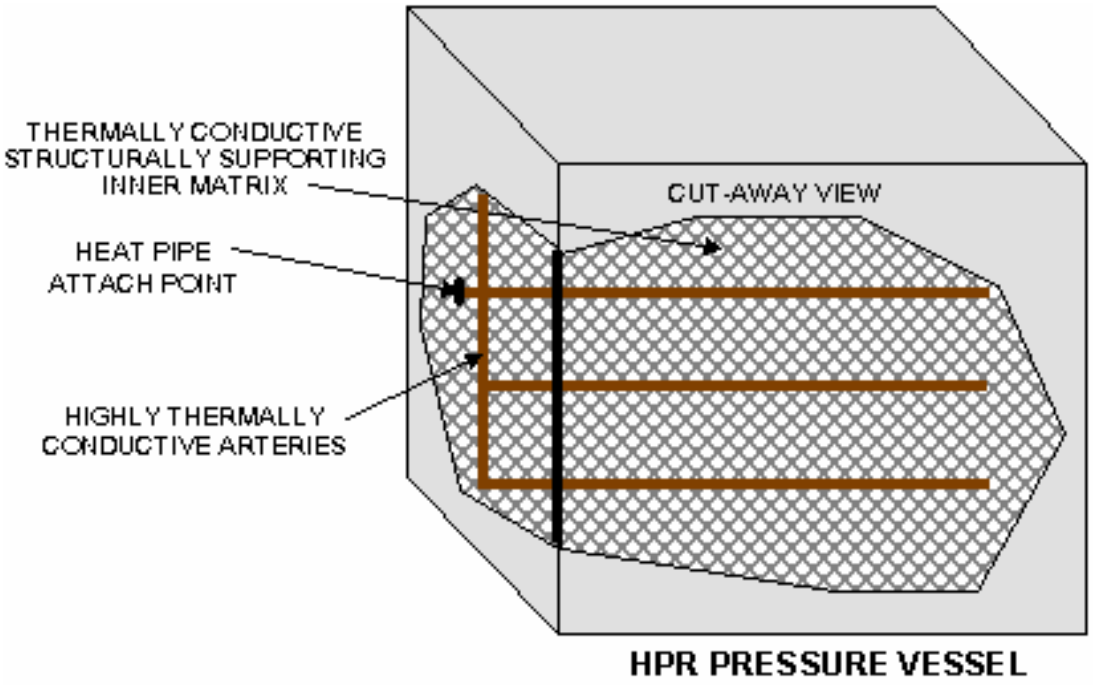

Figure 6.4: HPR Pressure Vessels Configured for Transcryogenic Gas Storage Might also Include the Use of Highly Thermally Conductive Arteries

Figures 6.5 through 6.10 illustrate one possible version of the basic Transcryogenic Gas Storage Process. For purposes of visual clarity, valves, regulators, and various pipe fittings have been omitted and simply represented by a line connecting the top of the HPR Pressure Vessel.

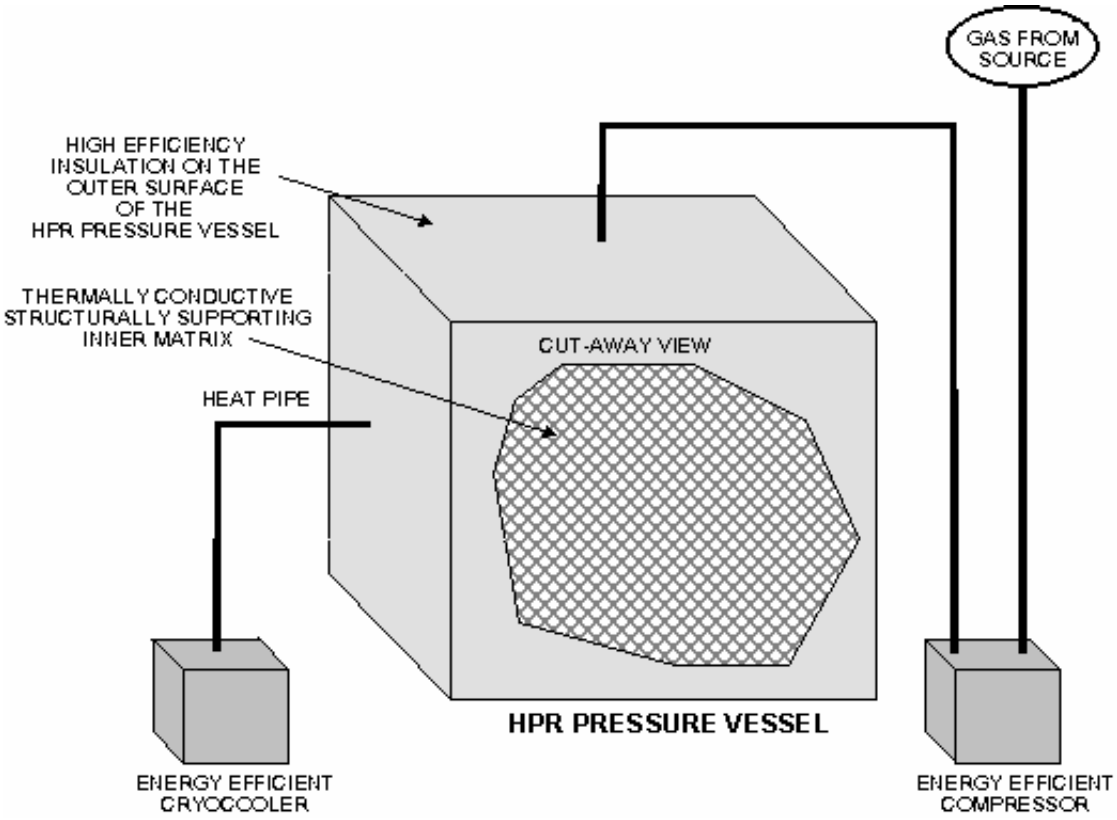

Figure 6.5: Empty HPR Pressure Vessel Configured for Transcryogenic Storage

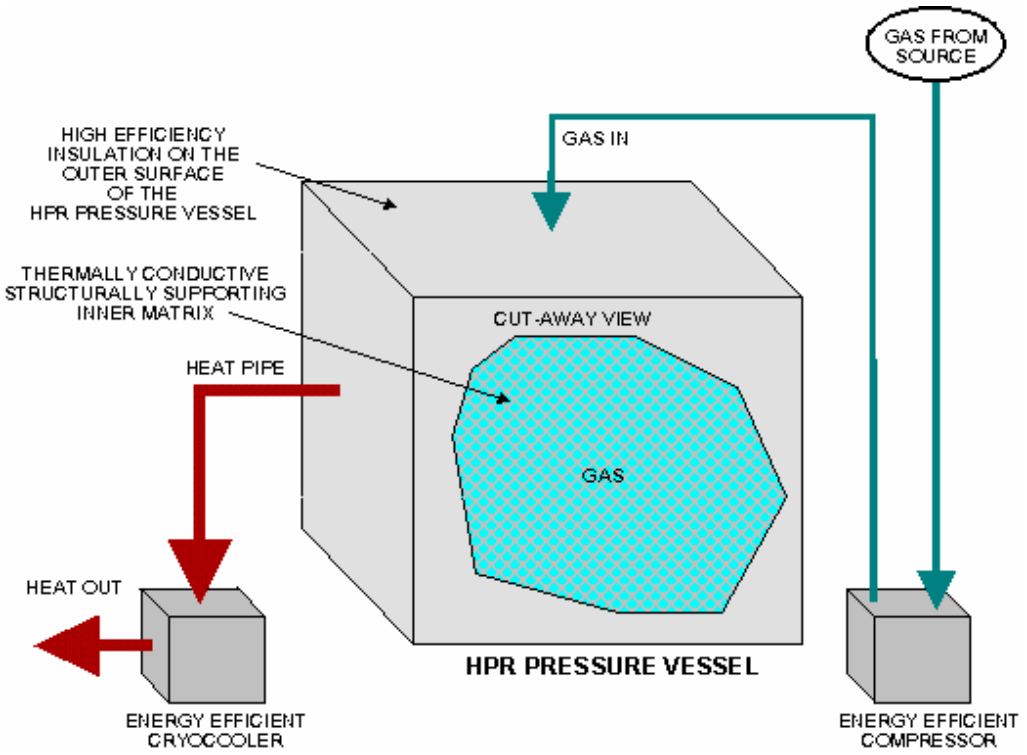

Figure 6.6: Gas is Compressed at Low to Moderate Pressure & Heat is Removed

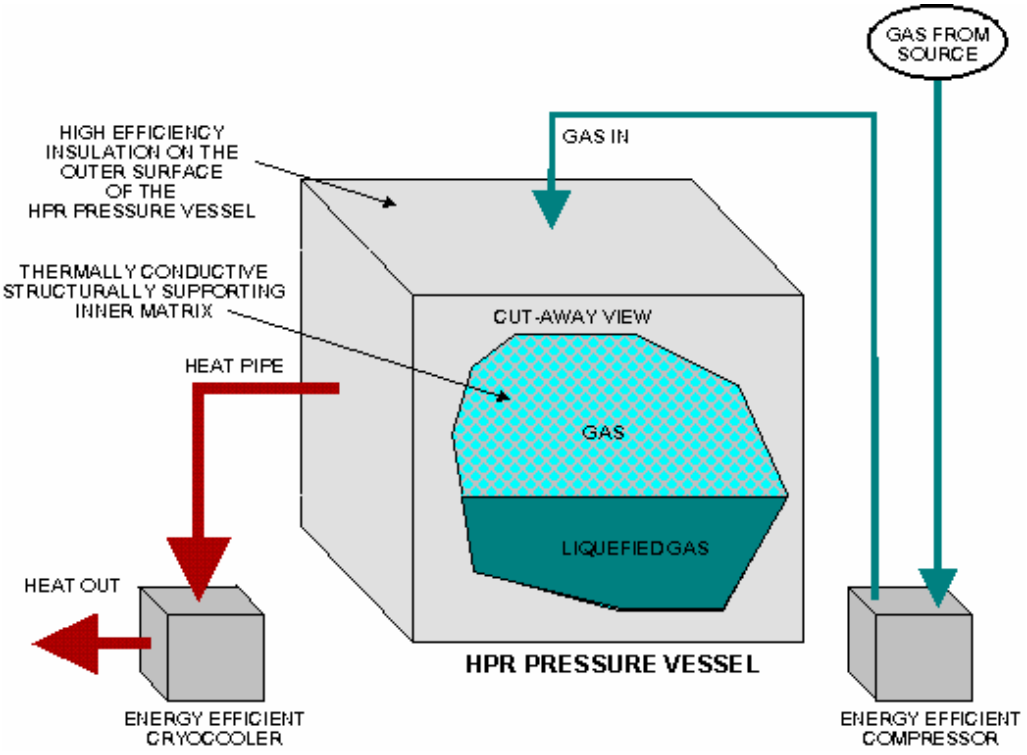

Figure 6.7: Gas Becomes Liquefied as Heat is Removed and Pressure is Increased

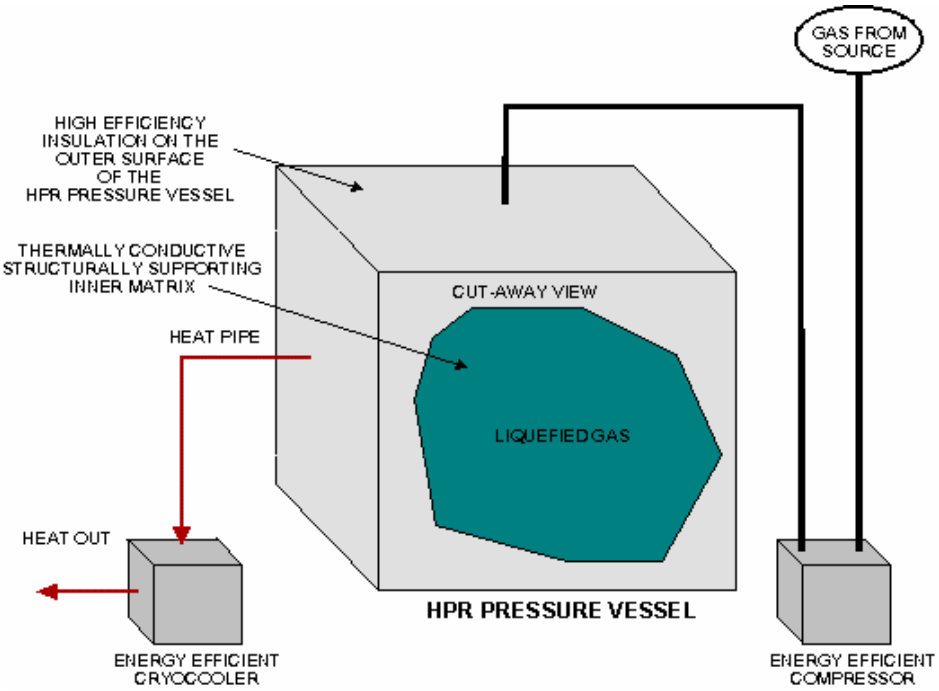

Figure 6.8: Filling Continues Until the HPR Pressure Vessel is Nearly Full of Liquefied Gas On-Demand Maintenance Level of Heat Removal Continues

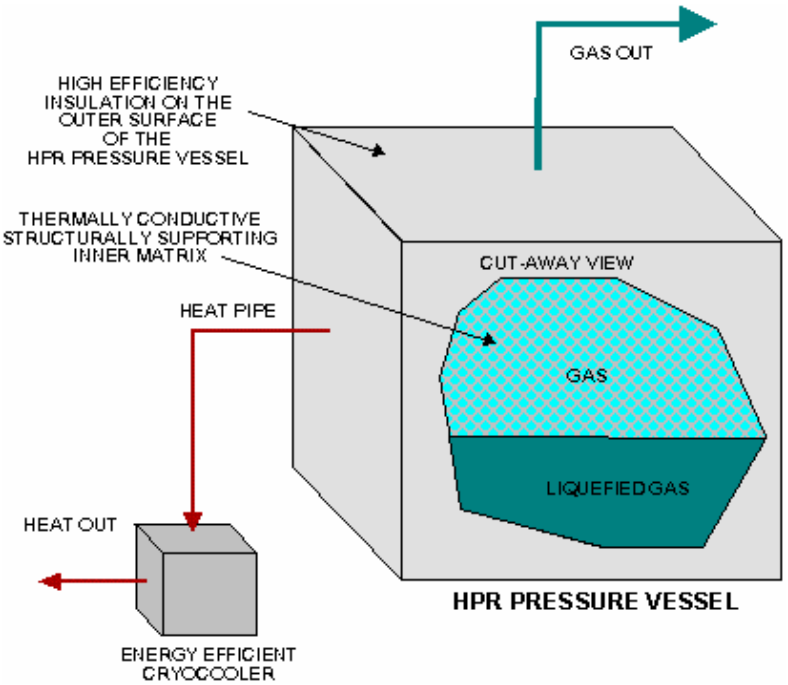

Figure 6.9: Gas is Removed by the User from the Top of the HPR Pressure Vessel On-Demand Maintenance Level of Heat Removal Continues

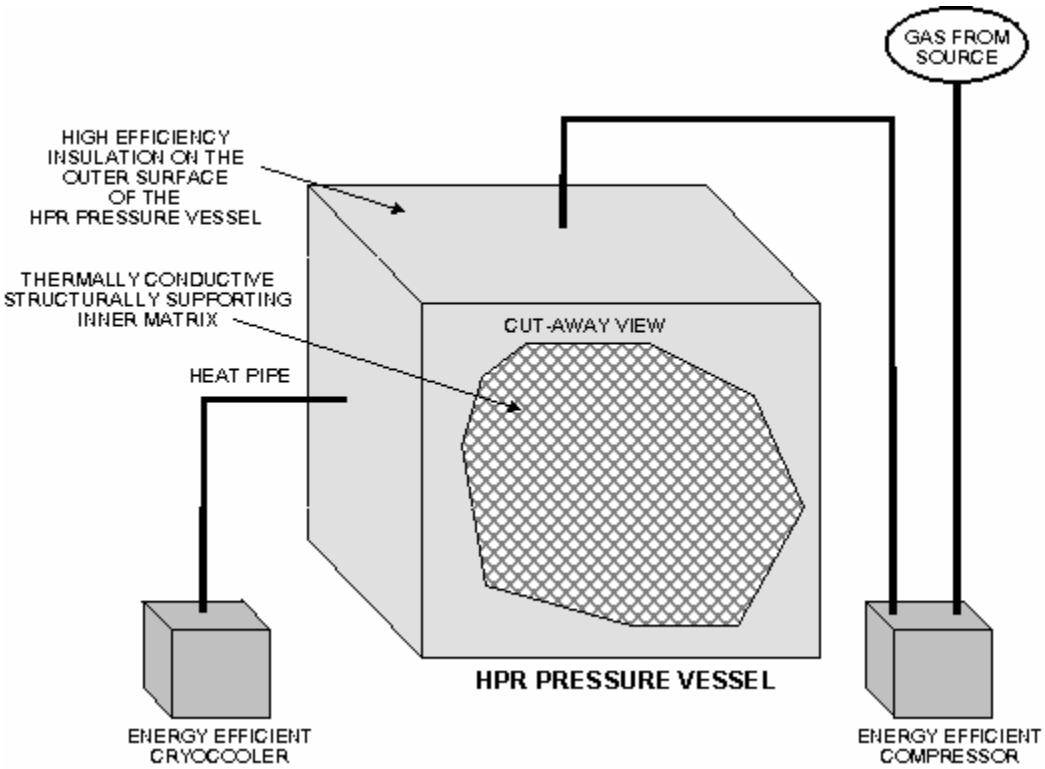

Figure 6.10: Empty HPR Pressure Vessel is Ready for Transcryogenic Refilling

CHAPTER 7. POTENTIAL APPLICATIONS FOR HPR™

7.1 Conventional Pressure Vessel Replacement

There are numerous applications for HPR™ pressure vessels in the commercial market place as direct replacements of conventional pressure vessels. Industrial pressure vessels, such as acetylene and oxygen tanks commonly used for welding, could be fabricated in the shape of a suitcase with the regulator safely recessed in a premolded cavity. These suitcase shaped tanks could be easily stacked onto pallets for convenient storage and handling. Medical oxygen tanks could be custom designed to incorporate human factors. Breathing air packs used by fire fighters could be shaped conformally to reduce possible obstructions. Scuba tanks could be more aerodynamically shaped. Additionally, cryogens could be conveniently stored indefinitely in actively cooled isothermal containers of any shape.

7.2 Automotive Fuel Tanks

This new technology is potentially useful for designing and fabricating automotive fuel tanks for pressurized gaseous fuels. This new and improved technology would allow for designing and manufacturing pressurized fuel tanks of any shape so as to make maximum use of limited available physical envelopes. This new technology has the additional potential benefit of producing pressurized fuel tanks which are less likely to fail catastrophically than equivalent conventional cylindrical pressure vessels due to the use of an improved approach for structural material distribution. Until HPR™, conventional cylindrical pressure vessels had been the only reasonable option available

for storing gaseous fuels on automobiles. However, due to their cylindrical shape, these tanks have been very difficult to efficiently fit on passenger cars. Most often these cylinders have been located in the trunk, which has had a negative impact on customer acceptance. Conformally shaped HPR^{TM} fuel tanks are ideal for storage of gaseous fuels on passenger cars where space and safety considerations are very important. HPR^{TM} fuel tanks for either Compressed Natural Gas (CNG), Liquefied Petroleum Gas (LPG), or Hydrogen (H2) could be direct replacements for the conventional gasoline tank. Further, additional tanks could be located in tight fitting formally unusable spaces to give passenger cars a conveniently long range between fill-ups. Of course, there would be no reason to locate HPR^{TM} fuel tanks in the trunk, leaving this space for the customer's use. All gaseous fueled automobiles, whether conventional, hybrid, or fuel cell, will be more acceptable to the customers if they are equipped with HPR^{TM} fuel tanks. This will translate into greater customer satisfaction, and ultimately greater market share. Figures 7.1 through 7.3 illustrate the HPR^{TM} advantage.

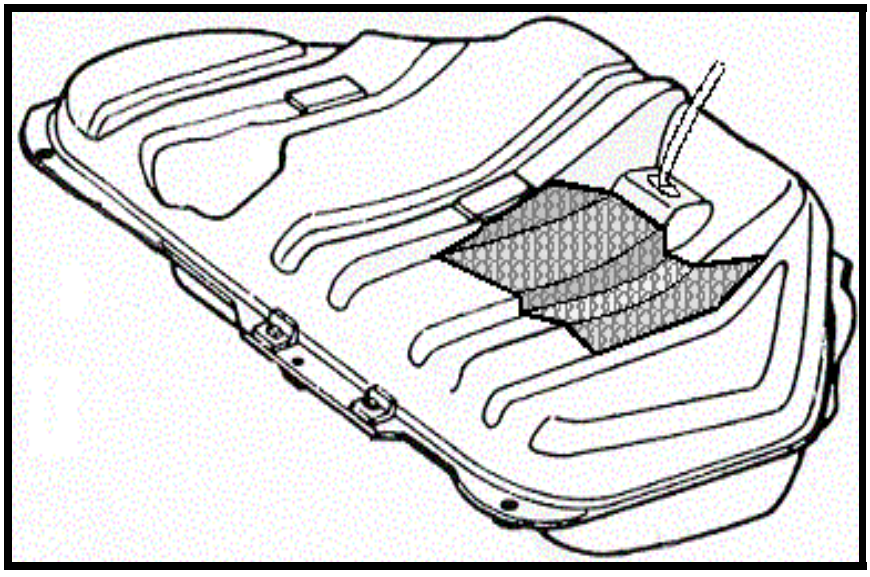

Figure 7.1: HPR^{TM} for Retrofit

Figure 7.2: HPR™ for Integrated Design

Figure 7.3: Cylinder Tanks of the Past

7.3 Aerospace Vehicular Tankage

In the particular case of aerospace vehicular tankage where weight conservation is very important; the weight savings associated with enhanced material efficiency combined with the weight savings associated with pressurized tanks integrated as structural members will amplify the value of the new technology. In addition, where cryogens are used, the isothermal characteristic of these tanks will reduce ullage. Therefore, cryogenic fuel and oxidizer will be more efficiently utilized on vehicles with HPR^{TM} tankage. This will all translate into dramatically increased agility, greater payload capacity, and lower operational costs. In brief, aerospace vehicles incorporating HPR^{TM} will be smaller, lighter, and have higher performance than those without it.

7.4 Portable Charge Cartridges

HPR^{TM} is a potential technology for fabricating rechargeable energy storage cartridges for pressurized gaseous fuels. HPR^{TM} could allow for designing and manufacturing charge cartridges of any size and shape so as to make maximum use of limited available physical envelopes. HPR^{TM} has the additional potential benefit of producing pressurized energy storage cartridges which hold more fuel and are less likely to fail catastrophically than equivalent conventional cylindrical pressure vessels due to the use of an improved approach for structural material distribution. Replacement of battery packs by fuel cells on future portable appliances such as portable power tools, lap-top computers, cell-phones, and VCR camcorders represents a very large potential market for HPR^{TM} charge cartridges. Micro-sized fuel cell systems have already

demonstrated energy storage densities three times greater than current battery-packs; with energy densities ten times greater being projected for the near future. Battery-pack sized Charge cartridges fabricated with HPR™ technology could provide very dense energy storage of gaseous fuels such as LP gas, natural gas, or pure hydrogen, for use in these appliances. These HPR™ charge cartridges could be quickly and safely recharged at home with wall mounted fixtures attached to fuel sources (similar in appearance to plug-in battery-pack chargers available today.). These wall mounted recharging units could even reform commercially available fuels such as propane or natural gas into pure hydrogen for storage in HPR™ charge cartridges, thus eliminating the need for a fuel reformer on each portable appliance. This would reduce product costs and leave more space for fuel. All fuel cell powered portable appliances which are also equipped with HPR™ charge cartridges will cost less and last longer between charges than those without them. Figures 7.4 and 7.5 illustrate the HPR™ concept.

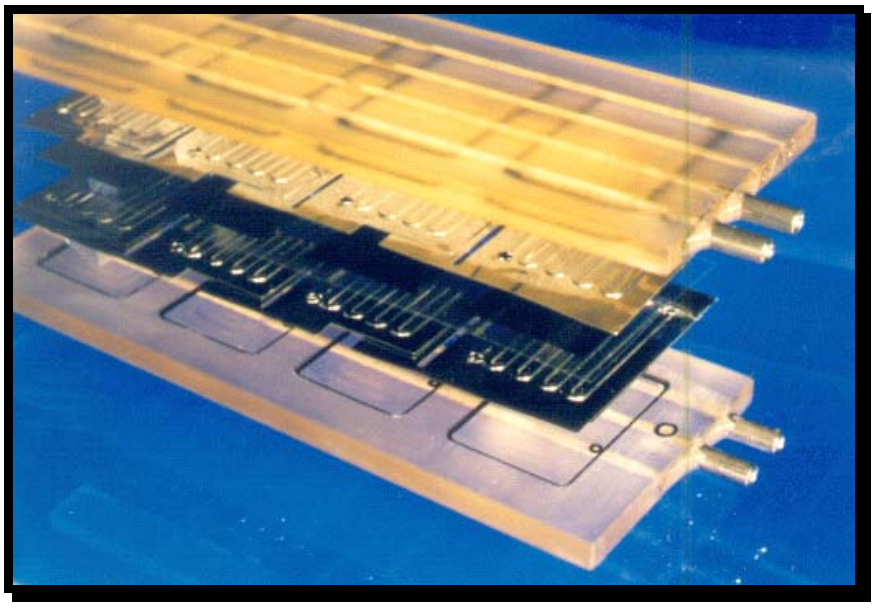

Figure 7.4: Energy Conversion with Micro Fuel Cells

Figure 7.5: Energy Storage in HPR™ Charge Cartridges

7.5 Automotive Crash Shields

In order to increase the crash worthiness of automobiles, manufacturers are evaluating the use of aluminum foam crash boxes integrated into their vehicular structures to absorb a substantial portion of any collisions [35]. Figure 7.6 shows a segment of an aluminum foam crash box shaped to fit on the side of a car. The energy absorption characteristics of aluminum foam undergoing compressive failure are uniquely compatible with the objective of protecting the passenger compartment. It would be an easy modification to make each of the aluminum foam crash boxes into HPR™ pressure vessels, and to fill them with a gaseous fire retardant. Upon impact the aluminum foam crash boxes would serve a dual purpose; absorbing the crash energy, and releasing fire retardant in the specific areas of the crash.

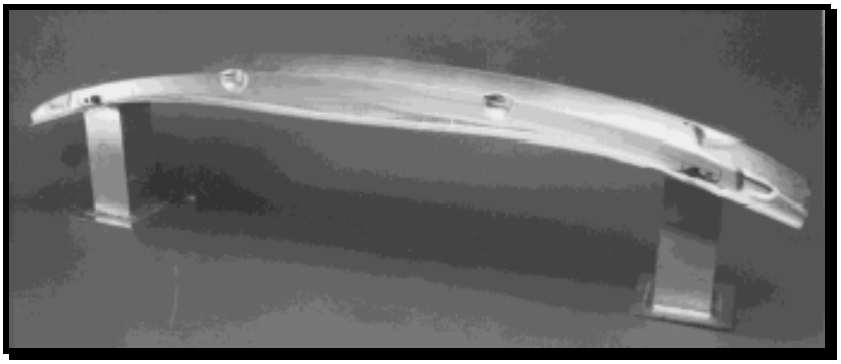

Figure 7.6: Aluminum Foam Crash Box Section [35]

7.6 Foam Core Civil Engineering Structural Members

Aluminum foam core structural members and fascia could be manufactured as HPR^{TM} pressure vessels filled with fire retardant for use as structural members and fascia on and in all civil engineering projects, including large buildings and skyscrapers (see Figures 7.7 and 7.8 below). These aluminum foam core structural members and fascia manufactured as HPR^{TM} pressure vessels filled with fire retardant would serve all the conventional functions that conventional building structural members and fascia serve along with serving as a fire fighting impact shield. In addition, these structural members and fascia would exhibit extremely high strength to weight, and stiffness to weight ratios, and accordingly high resonant frequencies, further enhancing their value on civil engineering projects. From both a practical and liability standpoint, all future construction projects would benefit from such an application.

Figure 7.7: The Sears Tower

Figure 7.8: The World Trade Center (inoblitus perpetuitatem)

REFERENCES

[1] Korner, C. and Singer, R., (2000), *Processing of Metal Foams – Challenges and Opportunities*, Advanced Engineering Materials 2000, 2, No. 4, pp 159 – 165.

[2] Zhou, J., Shrotriya, P. and Soboyejo, W., *Mechanisms and Mechanics of Compressive Deformation in Open-Cell Foams, Part I: Experements*, Priceton Materials Institute, and Department of Mechanical and aerospace Engineering, Priceton University, Priceton, NJ 08544.

[3] Young, W. and Budynas, R., (2002), *Roark's Formulas for Stress and Strain 7th Edition*, p. 520.

[4] Gerhard, H., *US patent number 4,840,282: Pressure-Resistant Tank*, Granted on 20 June 1989.

[5] Nishimura, Y., Kobayashi, T., Shingo, S. and Minoru, O, *US patent number 5,758,796: Pressure Vessel*, Granted on 02 June 1998

[6] Schoo, R., *US patent number 5,462,193: Composite Pressure Vessel*, Granted on 31 October 1995.

[7] Steele, R. and Stenger, R., *US patent number 5,647,503: Tank For Storing Pressurized Gas*, Granted on 15 July 1997.

[8] Giamei, A., (1997), *Aero-Engine and Naval Applications for Ultra-Lightweight Metals*, Proceedings of the Fraunhofer USA Metal Foam Symposium, Stanton, Delaware, 7 – 8 October, 1997.

[9] Falk, I. and Carlsson, T, *US patent number 5,564,587: Pressure Container*, Granted on 15 October 1996.

[10] Adderley, C., Fowler, J., Banks, S. and Boardman, J., *US patent number 5,323,953: Pressurized Storage For Gases*, Granted on 28 June 1994.

[11] Stannard, J., *US patent number 4,946,056: Fabricated Pressure Vessel*, Granted on 07 August 1990.

[12] Blair, M., Kunz, R., Warner, M., Davis, K., Wolcott, R., Turner, D. and Bennett, J., US patent number 5,577,630: Composite Conformable Pressure Vessel, Granted on 26 November 1996.

[13] *Technical Manual for Stabilized Aluminum Foam*, (2003), The Cymat Corporation, 6320-2 Danville Road, Mississauga, Ontario, Canada.

[14] *DUOCELL Aluminum Foam*, (2000), ERG Materials and Aerospace Corporation, 900 Stanford Avenue, Oakland California 94608.

[15] Banhart, J. and Baumeister, J., (1998), *Deformation characteristics of metal foams*, Journal of Materials Science, vol 33, pp 1431-1440.

[16] *Divinycell H*, (2002), Divinycell International AB, 315 Seahawk Drive, DeSoto, Texas 75115.

[17] Eric W. Weisstein. "*Sphere Packing*" From MathWorld--A Wolfram Web Resource. http://mathworld.wolfram.com/SpherePacking.html (retrieved April 2004).

[18] Eric W. Weisstein. "*Kepler Conjecture*" From MathWorld--A Wolfram Web Resource. http://mathworld.wolfram.com/KeplerConjecture.html (retrieved April 2004).

[19] Hales, T., "*The Kepler Conjecture*", http://www.math.pitt.edu/~thales/kepler98/ (retrieved April 2004).

[20] Eric W. Weisstein. "*Cube*" From MathWorld--A Wolfram Web Resource. http://mathworld.wolfram.com/Cube.html (retrieved April 2004).

[21] Chen, S., Devachetty, S and Mehta, B., *Hydrostatic Pressure Retainment (HPR) Tanks – Design and Analysis*, October 2002 (unpublished).

[22] *The BOC Group Results*, http://www.boc.com/news/article_detail.cfm?ID=640, Retrieved in April 2004.

[23] The Fraunhofer-Gesellschaft, http://www.fraunhofer.de/english/company/index.html, Retrieved in April 2004.

[24] Baumeister, J. and Hartmut, S., *US patent number 5,151,246: Methods forManufacturing Foamable Metal Bodies*, Granted on 29 September 1992.

[25] *Foaminal Properties Overview and Design Guide*, Fraunhofer Institute Manufacturing and Advanced Materials, Wiener Strasse 12, 28359 Bremen, Germany.

[26] Dougill, B., Garrett, M. and Green, J., (1998), *Metal Foam Porosity - Test Report*, BOC Gases Fabrication Technology Centre, Lower Walsall Street, Wolverhampton, W. Midlands, United Kingdom.

[27] Dougill, B., Garrett, M. and Green, J., (1998), *Bursting Pressure Tests of Aluminum Foam Blocks - Test Report*, BOC Gases Fabrication Technology Centre, Lower Walsall Street, Wolverhampton, W. Midlands, United Kingdom.

[28] Eifert, H., *HPR Technical Report*, (1998), Fraunhofer Resource Center - Delaware, 501 Wyoming Road, Newark, Delaware, Delaware 19716.

[29] Dougill, B., Garrett, M. and Green, J., (1999), *Metal Foam Porosity - Test Report*, BOC Gases Fabrication Technology Centre, Lower Walsall Street, Wolverhampton, W. Midlands, United Kingdom.

[30] Dougill, B., Garrett, M. and Green, J., (1999), *Bursting Pressure Tests of Aluminum Foam Blocks - Test Report*, BOC Gases Fabrication Technology Centre, Lower Walsall Street, Wolverhampton, W. Midlands, United Kingdom.

[31] Eifert, H., *HPR Technical Report*, (2000), Fraunhofer Resource Center - Delaware, 501 Wyoming Road, Newark, Delaware, Delaware 19716.

[32] Dougill, B., Garrett, M. and Green, J., (2000), *Porosity & Bursting Pressure Tests of Aluminum Foam Blocks - Test Report*, BOC Gases Fabrication Technology Centre, Lower Walsall Street, Wolverhampton, W. Midlands, United Kingdom.

[33] Wadley, H., (2002), *Cellular Metals Manufacturing*, Advanced Engineering Materials 2002, 4, No. 10, pp 726 – 733.

[34] Wadley, H., (2000), *Properties and Applications of CastAluminum Sponges*, Advanced Engineering Materials 2000, 2, No. 4, pp 188 – 199.

[35] Wadley, H., (2000), *Aluminum Foam for Automotive Applications*, Advanced Engineering Materials 2000, 2, No. 4, pp 200 – 204.